PRECISION DETERMINATION OF THE ENERGY RELEASED IN NUCLEAR REACTIONS IN THE LIGHT ELEMENTS

Thesis by

Alvin V. Tollestrup

In Partial Fulfillment of the Requirements

For the Degree of

Doctor of Philosophy

California Institute of Technology

Pasadena, California

1950

ACKNOWLEDGMENTS

It is with much gratitude that I acknowledge the active assistance and many helpful suggestions given by Professors C. C. Lauritsen and W. A. Fowler. I also wish to thank Professors R. F. Christy and T. Lauritsen for valuable advice and consultations. I would also like to express my appreciation to my wife, Alice Tollestrup, for typing this manuscript. This work was assisted by the joint program of the ONR and AEC.

ABSTRACT

A precision determination of the energy released in the following nuclear reactions has been made: (1) $Be^9(p,\alpha)Li^6$, (2) $Be^9(p,d)Be^8$, (3) $Be^8(\alpha)He^4$, (4) $D(d,n)He^3$, (5) $D(d,p)H^3$, (6) $Li^6(p,\alpha)He^3$, (7) $B^{10}(p,\alpha)Be^7$. An electrostatic generator and analyzer was used to furnish a beam of protons of accurately known energy and a double focusing magnetic spectrograph used to perform a momentum analysis of the particles arising in the reactions. A scintillation counter suitable for the detection of particles arising in nuclear reactions is described and the theory of the associated electronic equipment is given. The Q-values of the reactions are used to calculate the $n^1 - H^1$ mass difference and three low energy points on the range energy curve are established. A resume of all accurately determined Q-values is given.

TABLE OF CONTENTS

LIST OF FIGURES

PART I

INTRODUCTION

The determination of the amount of energy released in a given nuclear reaction is one of the primary problems of nuclear physics. In the past few years experimental techniques have advanced to the point where the errors in these measurements have decreased by approximately a factor of ten. This yields a number of interesting results.

First, the determination of nuclear Q-values enables one to calculate the masses and mass defects of the elements. A comparison with the mass spectroscopic data thus yields a direct verification of the Einstein relation $E = mc^2$. On the other hand assuming this relation to be correct a second method is available for the computation of nuclear masses. It should be observed that the mass of the neutron is obtainable only from nuclear data and a portion of this investigation is concerned with determining that value.

The second result of the more accurate Q-values is a revision of the Range-Energy relation for charged particles in the low energy region. The original data used in fixing this relationship came from natural α-particles whose energy had been accurately measured by determining their radii of curvature in a uniform magnetic field. These α-particles have an energy of the order of 5 Mev. To obtain the low energy data of the Range-Energy curve, these natural α-particles were slowed down by interposing various thicknesses of matter. This method was not very accurate and left the low energy portion relatively uncertain. A better method of obtaining this data consists of measuring the ranges of particles emitted in a nuclear reaction with a small, accurately known Q-value. Three new points on the Range-Energy relation may be established from

the Q-values here studied.

Finally, accurate values for the binding energy of the various nuclear isotopes are of considerable theoretical importance. The H^2, H^3, and He^3 problems, the β-decay of the neutron, and the problem of nuclear forces all require this data.

The electrostatic accelerator and analyzer previously described [1] were used to obtain monenergetic protons. The new double focusing magnetic spectrograph [2] was used to analyze the charged particles emitted in the reaction under study. The high energy resolution of this instrument allows the energy of the particles to be determined very accurately and simultaneously frees the results of any errors in the Range-Energy relation. The detector used in conjunction with the spectrograph was a scintillation counter which will be described in detail later.

The following reactions were studied:

(1). $Be^9 + H^1 \rightarrow Li^6 + He^4 + Q_1$

(2). $Be^9 + H^1 \rightarrow Be^8 + D + Q_2$

(3). $Be^8 \rightarrow 2He^4 + Q_3$

(4). $D + D \rightarrow n^1 + He^3 + Q_4$

(5). $D + D \rightarrow H^1 + H^3 + Q_5$

(6). $Li^6 + H^1 \rightarrow He^3 + He^4 + Q_6$

(7). $B^{10} + H^1 \rightarrow He^4 + Be^7 + Q_7$

Be^8 is not a naturally occurring isotope and it had long been suspected that it was unstable to decay into two α-particles. Several measurements [3,4] have been made of the amount of energy

released in this disintegration with divergent results. Reactions (1), (2), (3) allow this energy to be accurately determined.

The mass difference between the neutron and atomic hydrogen may be obtained by subtracting equation (4) from equation (5):

$$n^1 - H^1 = (H^3 - He^3) + (Q_5 - Q_4). \qquad (8)$$

The $(H^3 - He^3)$ difference has been accurately determined [5,6] from the β decay of H^3. Thus by measuring Q_4 and Q_5, the $n^1 - H^1$ value may be determined. This is found to be considerably higher than the old value and is in good agreement with other recent determinations of this value.

Reactions (6) and (7) lead to three new points on the Range-Energy curve in the low energy region.

PART II

APPARATUS

A diagram of the experimental arrangement is given in Fig. 1. The protons from the electrostatic generator were analyzed in the electrostatic analyzer and directed onto the target. The particles arising in the reaction and emitted into the angular sector $\Theta \pm \Delta\Theta$ entered the double focusing spectrograph and were focused upon the entrance to the scintillation counter detector. The angular resolution of the spectrograph is shown in Fig. 2. This curve was obtained by moving across the spectrograph opening a beam of elastically scattered protons collimated by a very narrow slit. Considerably greater angular resolution is obtainable from the instrument, but in view of the weak intensity of some of the reactions studied, the maximum angular opening of the instrument was deemed necessary in most cases.

The energy E of a particle of rest mass M_0, and momentum P is given by

$$E = \sqrt{P^2c^2 + (M_0c^2)^2} - M_0c^2 \tag{9}$$

The momentum of a particle with a radius of curvature ρ, charge Ze, and moving in a field B is given by

$$P_c = Ze B\rho \tag{10}$$

Substituting into Eq. (9) and expanding, it is found

$$E = M_0c^2\left\{\sqrt{1 + \left(\frac{Be Z\rho}{M_0c^2}\right)^2} - 1\right\} \tag{11}$$

$$\approx \frac{(Be Z\rho)^2}{2M_0c^2}\left[1 - \frac{1}{4}\left(\frac{Be Z\rho}{M_0c^2}\right)^2 + \cdots\right]$$

Defining E_o to be the non-relativistically calculated energy, one has

$$E_o = \frac{(Be Z\rho)^2}{2 M_o c^2} \tag{12}$$

and substituting into Eq. (11) there results

$$E \approx E_o \left[1 - \frac{E_o}{2 M_o c^2} \right] \tag{13}$$

The term in brackets is the relativistic correction and amounts to at most 0.2%. A similar calculation for the electrostatic analyzer gives Eq. (13) also except that the sign in parenthesis is plus.

The field B and radius ρ were not measured, but a magnetometer was used which measured the relative values of B [7]. This consisted of a coil carrying a current I suspended in the magnetic field between the pole faces of the spectrometer. The coil had a restoring torque furnished by a spring which just balanced the torque due to the field acting on the coil. Thus we have

$$BI = \text{a constant} \tag{14}$$

Substituting into Eq. (12),

$$E_o = \frac{Z^2}{M_o} \frac{C_m}{I^2} \tag{15}$$

where C_m is the magnetic constant which was determined by calibrating the magnetic field on particles of known energy in a manner to be described later, and Z and M_o are measured in units of proton charge and mass. The current I was measured with a potentiometer and precision resistor and is labeled millivolts on curves shown later.

PART III

SCINTILLATION COUNTER

The particles from the target reaction are analyzed and focused upon the detector by the double focusing magnetic spectrograph. A suitable detector for these particles should have the following properties:

a) The sensitive volume should be connected directly onto the vacuum chamber of the spectrograph. All gas filled detectors (e.g. Geiger counter or proportional) require a thin window through which the charged particles must pass. This defines a low energy limit, which is a function of the particle charge and beyond which the detector is useless.

b) The response should be proportional to the energy of the particle. Since the spectrograph makes essentially a momentum analysis, groups of interfering particles can be separated if the detector is energy sensitive.

c) The dead time of the detector should be of the order of 20 μ sec. or less if the correction to the counting rate is to be less than 1% at the rates encountered in this application.

d) The signal to noise ratio should be high for particles whose energy is 100 Kev or more. Also microphonics should not be troublesome.

e) The detector should be insensitive to the stray magnetic field of the spectrograph which in this case is of the order of 1000 oersteads.

The scintillation counter as it has finally been developed meets conditions (a), (c), (d) and (e). Condition (b) is not satisfied very well, and methods to circumvent this disadvantage were developed and will be described later.

Fig. 3 shows the construction of the device and is essentially the form developed in Ref. (8). The particles enter through the 5/16" hole of the hemispherical mirror located about 3" behind the focal point of the spectrograph and strike the ZnS phosphor on the end of the Lucite pedestal.* The resulting light is transmitted via the mirror through the Lucite window and brought to focus upon the cathode of the electron multiplier tube. The Lucite window is sealed into the brass tube with a neoprene gasket and held in place by friction. The light escaping from the back of the screen is roughly collimated by the Lucite pedestal. The mirror was constructed by cutting the top off a 7 1/2 watt, 110 volt lamp, drilling a 5/16" hole, and coating the inside surface with aluminum.

The characteristics of the electron multiplier tube are given in Ref. (9). In addition three properties have been investigated. The sensitive area of the cathode of the tube was investigated by allowing light to fall upon different portions of the cathode and plotting the response of a microammeter connected to the output of the

---

* For high resolution a slit should be placed at the focal point of the spectrograph. The hole in the mirror is large enough to permit all the particles that form an image of the target spot to enter the detector.

tube. The results are given in Fig. 4. The cathode is 0.5" X 1" and it is seen from the curve that the sensitive width of a typical cathode is only 1/8" and is located near the innermost edge of the cathode. The length of the sensitive area similarly was found to be about 3/4". The small size of the sensitive area and its location make the problem of an efficient optical system very difficult to solve.

A suitable system for selecting the tubes with the best signal to noise ratio was also sought. The noise arises from two sources. First, the work function of the photo-cathode is low enough so that an appreciable number of thermionic electrons are emitted even at room temperature. And second, the leakage currents due to the high voltages employed contribute to the noise spectrum. There are very large variations in these two sources of noise from tube to tube. Consequently a light tight box was constructed and a 1/4 watt neon tube was mounted in such a way as to let light into the box through a pin hole. The neon tube was connected into a simple relaxation oscillator circuit and the resulting flashes of light were used as a standard signal source to compare with the noise pulses of a series of 931-A electron multiplier tubes. The high voltage was varied and the signal to noise ratio observed. The signal to noise ratio was plotted against signal height in order to compare various tubes at the same gain. (This was necessary since the gain of different 931-A tubes varies by a factor of 100 from tube to tube at a given high voltage. Thus the light input was assumed to be constant and the signal output was taken as a measure of tube gain.) Fig. (5) shows a typical curve

obtained and it is to be noted that the signal to noise ratio is constant up to a given high voltage and then decreases rapidly. The signal to noise ratio here plotted is peak signal to peak noise. Some tubes observed were 100 times worse than the one shown.

Both the 1P28 and 1P21 electron multipliers were tested. The 1P28 has a special ultra violet light transparent envelope and the 1P21 is a 931-A that the manufacturer has selected for high signal to noise ratio and sensitivity. The best 1P28 seemed to be slightly better in actual use than the best 931-A. It was found necessary to discard some 1P21's and the best one found appeared no better than the best 931-A. Since the price of the 1P21 is five times that of the 931-A it does not seem desirable to use this tube.

The distribution of voltage on the various electrodes was investigated to determine its effect on the signal to noise ratio. The operation of the tubes with 50% more voltage on the last 3 electrodes appears to improve the signal to noise ratio by a factor of 2 above that obtained by distributing the voltages equally. Painting the envelope of the tubes with Aquadag and connecting it to the third dynode generally improved the signal to noise ratio.

Finally the reaction of the tube to a magnetic field was investigated. A field of about 40 oersteads in an axial direction will completely cut the tube off, and one of only 10 oersteads will appreciably change the gain. The electrodes are made of magnetic material and the residual field in them was found to affect the gain of the tube after it was subjected to a strong field. The action of an axial field also depends upon the direction in which it acts, and it has the least effect

when it is directed from top to bottom in the tube. The field was measured in the region where the tube was to be placed and was found to have a maximum value of 1000 oersteads. A shield was constructed of two concentric 1/4" thick iron cylinders and a mu metal cylinder adjacent to the tube and is effective enough to reduce the field to less than 10 oersteads at the position of the tube.

A number of different phosphors were obtained and tested with Polonium α-particles. They were:

Patterson D Silver activated

#1410 Blue ZnS

#500 $CaWo_4$

#1900 Green ZnS

RCA type 33Z20 A

The type 1900 is copper activated and has a very long period phosphorescence associated with it which made it unsuitable. Calcium tungstate gave pulses only 1/10 that of the RCA 33Z20 A. The type D, #1410, and RCA ZnS phosphors all gave about the same size output pulses with the RCA being the faster. Moreover, when tried at proton energies of 100 Kev the most satisfactory phosphor was the RCA one, as the type D gave a very jagged and unreproducible pulse. The 33Z20 A is used in all the following work.

A histogram showing the distribution of grain size in the RCA phosphor was obtained by measurements with a low power microscope and is given in Fig. (6). It is seen that they cover a wide range of sizes. However, it is apparent that essentially all grains are 800 Kev

thick or more for protons and 2.4 Mev for α-particles. Thus some deviation in the shape of the light pulse distribution should be expected as the energy is increased to the point where the protons may completely pass through the grains.

The screens are prepared by dusting the phosphor upon the Lucite pedestal which has a thin film of grease on it. They are thus only one grain layer in thickness and the percentage area left uncovered by phosphor appears under a microscope to be less than 5% and could be decreased to zero by making the screen slightly thicker.

The optical system for gathering light from the phosphor and focusing it upon the photo-cathode was studied with the object of improving its light gathering properties. The size of the screen is fixed by the size of the focal spot of the spectrograph which is slightly less than 5/16" in diameter. However the sensitive area of the photo-cathode is 1/8 X 3/4" as shown earlier. The mirror forms an enlarged image of the screen on the cathode. The aberrations were investigated graphically and found to be so large that light from any portion of the screen can reach the sensitive area of the cathode. The light from some portions of the screen is much more effective than that from others and this is one of the sources of spread in pulse height observed from monoenergetic protons. It seems that the system used is about as effective as it is possible to make it in view of the type of construction employed in the 931-A. The solid angle through which light may enter the tube is limited to a sector of about 60° in the horizontal plane and 150° in the vertical. The new RCA type 5819 tube which has the cathode located behind a flat end-on window offers the possibility of

obtaining a much more efficient optical system.

Bias curves were measured for 5 Mev Po α-particles with no mirror, with a mirror and the back of the screen covered up, and finally in the normal operating condition. These are shown in Fig. (7).* Since the pulse heights are proportional to the amount of light falling on the photo-cathode, it is seen that the mirror contributes some 65% of the light and the back of the screen 35%. Several optical systems were tried in back of the screen in an attempt to increase the amount of light received from the back. Lens systems took up so much space that the distance from tube to screen had to be increased which diminished the light received via the mirror excessively. The most effective system was obtained by evaporating onto the back of the pedestal an aluminum mirror and placing the ZnS directly on top, but even this was less effective than leaving the back of the pedestal uncovered. This is due to the large scattering that must take place in transmitting light through the screen.

---

* A bias curve measures the number of pulses above a given voltage against voltage.

PART IV

AMPLIFIER

The associated equipment required is an amplifier to raise the pulse level from several millivolts up to 100 volts, a discriminator to differentiate between the background noise and the true pulses, and a regulated high voltage power supply for the 931-A. Fig. (8) shows the complete circuit. A complete discussion of such amplifiers is given in Ref. (10). However there are two pecularities of this type detector that must be taken into account in the amplifier design. First, the amplifier frequency response must be adjusted in order to obtain the maximum signal to noise ratio and second, the wave shape of the pulse going to the discriminator must be such that each pulse brings the discriminator above the firing point once and only once per pulse.

The signal to noise ratio problem will be considered first. From the curves shown in Fig. (5) it is seen that no significant variation in the signal to noise ratio takes place for variations of the high voltage below the sharp break in the curve. However, the noise from the amplifier must be added to that of the multiplier tube and therefore as the high voltage is lowered the signal decreases, the amplifier noise becomes greater than that of the multiplier, and the signal to noise ratio decreases. Consequently, for best signal to noise ratio the effect of the amplifier noise should be small. Since the RMS noise voltages combine as the square root of the sum of their squares, if the multiplier noise is 3 times that of the amplifier the total signal to noise ratio is within 5% of that of the tube alone.

In addition to adding noise to the signal, the amplifier can also affect the signal to noise ratio by means of its frequency response

characteristics. Light is emitted exponentially as a function of time from the phosphor and leads to a current pulse from the electron multiplier as shown below with a time constant of the order of 1 μsec. Noise

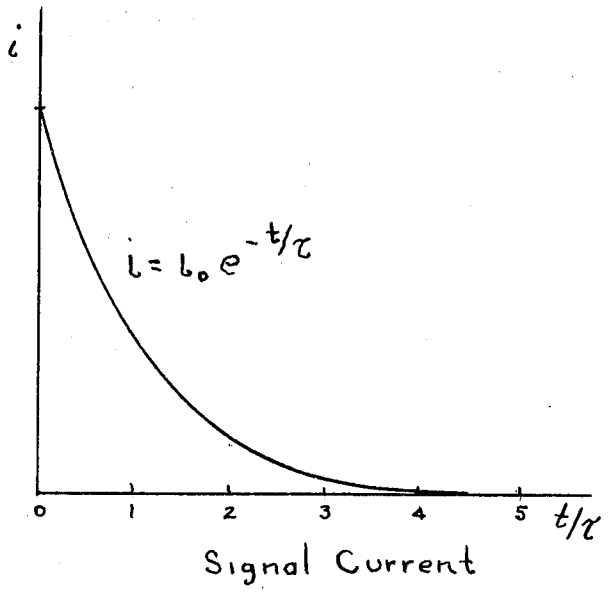

Signal Current

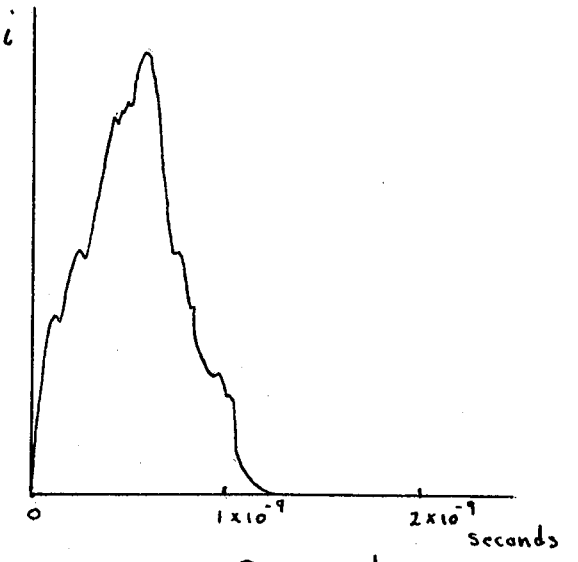

Noise Current

originates from single thermionic electrons leaving the photo-cathode and being multiplied some 10^6 times and giving rise to current bursts at the collector of the multiplier of less than 10^{-9} second duration as shown in the figure. These two current wave forms are integrated by means of the output capacity of the electron multiplier tube and if normalized to unity appear as shown below. (This assumes $\tau >> 10^{-9}$

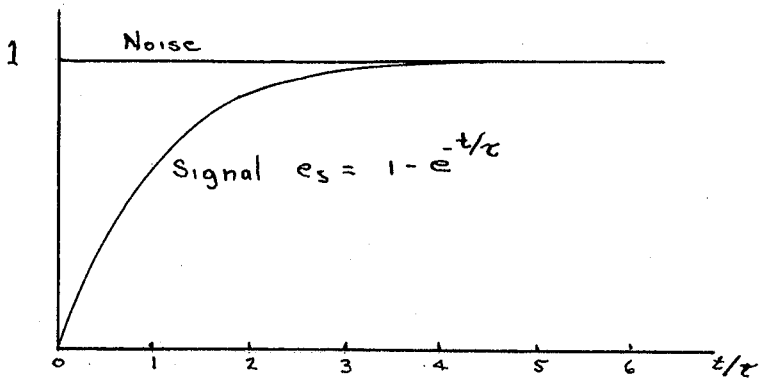

second, which is generally true.) These two pulses are then distorted

by an amplifier before being counted. The effect of the amplifier

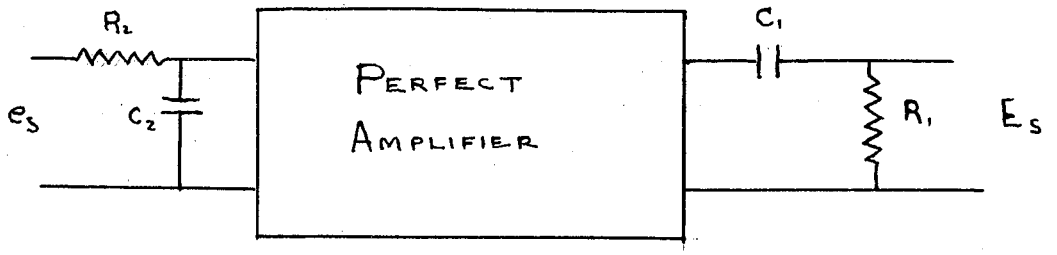

can be obtained by replacing it with a perfect one and adding two RC circuits. The circuit R_2C_2 duplicates the high frequency response and thus establishes a rise time $\tau_2 = R_2C_2$ for the amplifier, and the circuit R_1C_1 duplicates the low frequency response and hence differentiates the signals with a time constant $\tau_1 = R_1C_1$.

Before obtaining an exact solution, a few qualitative considerations are in order. First suppose $\tau_2 \simeq 0$. The circuit R_1C_1 then differentiates the noise and signal as shown. Obviously peak signal

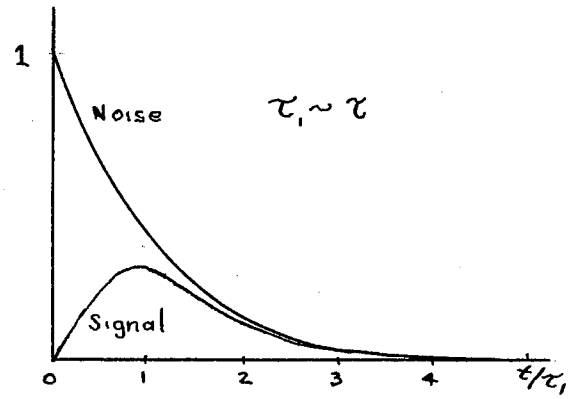

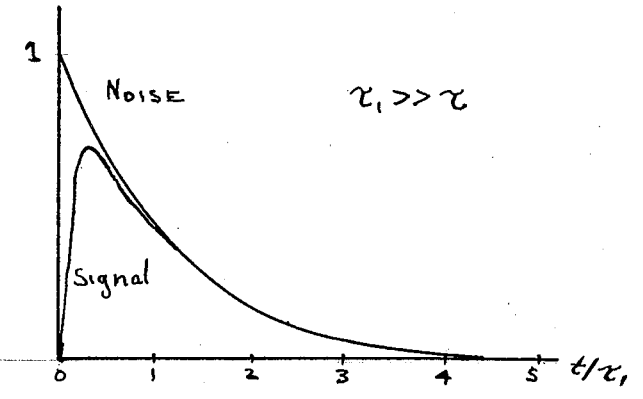

to peak noise ratio is seriously decreased in the case where $\tau_1 \sim \tau$ but little affected when $\tau_1 >> \tau$. Further insight into the question is obtained by considering the frequency spectrum of the noise and signal pulses. Since the wave forms coincide at values of $t > 4\tau$, the frequency spectrums must be identical for frequencies below $\frac{1}{4\tau}$ and above this frequency the noise spectrum must predominate. Thus if one sets $\tau_2 = 0$

and $\tau_1 \sim \tau$, the amplifier is passing only those frequencies for which the noise spectrum predominates over that of the signal and the signal to noise ratio is decreased. Any amplifier response limited exclusively to frequencies below $\frac{1}{4\tau}$ must give a signal to noise ratio of about 1. It is apparent that the signal to noise ratio can never be increased to greater than 1 by any amplifier design.

The exact solution is now worked out by the use of the Laplace transform. Considering the signal voltage as given by $e_s = 1 - e^{-t/\tau}$ and the noise voltage as a step function of unit height, we have for the Laplace transforms

$$\mathcal{L}[e_s(t)] = \frac{1}{s + 1/\tau} \quad ; \quad \mathcal{L}[e_n(t)] = \frac{1}{s} \tag{16}$$

The response of the amplifier is

$$G(s) = \frac{s/\tau_2}{(s + 1/\tau_1)(s + 1/\tau_2)} \tag{17}$$

The "signal out" is then given by

$$E_s(t) = \mathcal{L}^{-1}\left\{ \frac{1}{\tau\tau_2} \frac{s}{(s+\frac{1}{\tau})(s+\frac{1}{\tau_1})(s+\frac{1}{\tau_2})} \right\} \tag{18}$$

and the "noise out" is given by

$$E_n(t) = \mathcal{L}^{-1}\left\{ \frac{1}{\tau_2 (s+\frac{1}{\tau_1})(s+\frac{1}{\tau_2})} \right\} \tag{19}$$

The inverse transforms are found to be

$$E_S(t) = \frac{-\tau_1\tau_2 e^{-t/\tau_2}}{(\tau_1-\tau_2)(\tau-\tau_2)} + \frac{\tau\tau_1 e^{-t/\tau}}{(\tau_2-\tau)(\tau_1-\tau)} + \frac{\tau_1^2 e^{-t/\tau}}{(\tau_1-\tau_2)(\tau_1-\tau)} \qquad (20)$$

$$E_n(t) = \frac{\tau_1}{\tau_1-\tau_2}\left\{ e^{-t/\tau_1} - e^{-t/\tau_2} \right\} \qquad (21)$$

The signal to noise ratio is defined by

$$R = \frac{E_S|_{MAX}}{E_n|_{MAX}} \qquad (22)$$

E_N max is easily obtained by differentiation and if two parameters a and b are defined

$$a = \tau/\tau_1 \qquad b = \tau/\tau_2 \qquad (23)$$

we have

$$E_n|_{MAX} = \left(\frac{b}{a}\right)^{\frac{1}{1-b/a}} = \left(\frac{\tau_1}{\tau_2}\right)^{\frac{1}{1-\tau_1/\tau_2}} \qquad (24)$$

This equation indicates that the peak noise is a constant for a series of amplifiers in which the ratio of the upper to lower half power frequency is kept constant.

A similar solution for $E_S|_{MAX}$ is not possible in general. Consequently the equation was differentiated with respect to t for given values of a and b and the resulting transcendental equation solved for the time of the maximum. This was then substituted back into Eq. (20)

and $E_s|_{MAX}$ obtained. The solution for $b = \infty$ (an amplifier with perfect high frequency response), $b = 1$ (rise time of amplifier equal to the decay time of phosphor) and $b = 0$ was calculated for various values of a from 0 to 2. Also for $a = 1$ the solution was obtained for various values of b. The solution is facilitated if one defines

$$x = e^{-t/\tau} \tag{25}$$

which when substituted in Eq. (20) along with Eq. (23) gives

$$E_s = \frac{-bx^b}{(b-a)(1-b)} + \frac{bx}{(1-b)(1-a)} + \frac{bx^a}{(b-a)(1-a)} \tag{26}$$

This solution breaks down if $a = 1$ ($\tau = \tau_1$), $b = 1$ ($\tau = \tau_2$) or if $a = b = 1$ ($\tau = \tau_1 = \tau_2$). The appropriate special cases are

$$E_s(b=1) = \frac{x^a - (a-1)x\ln x - x}{(a-1)^2} \tag{27a}$$

$$E_s(a=1) = b\,\frac{x^b - (b-1)x\ln x - x}{(b-1)^2} \tag{27b}$$

$$E_s(a=b=1) = \tfrac{1}{2}x(\ln x)^2 \tag{27c}$$

The result of solving these equations for the signal to noise ratio is given in Fig. (9). It is seen that for $b = \infty$ it is necessary to differentiate with a time constant $\tau_1 \geq 50\,\tau$ in order to have $S/N \geq 0.9$. On the other hand by making the high frequency response of the amplifier

such that the rise time equals the phosphor decay time, $\tau_2 = \tau$ or $b = 1$, then it is feasible to differentiate with a time constant $\tau_1 = 3\tau$ and still have $S/N \geq 0.9$, but the pulses are of a much shorter duration, which means the counting rate can be made much higher. The curves are not plotted for other values of b, but their intercept with the line $a = 1$ is indicated and their approximate course is readily inferred.

In the above discussion it is assumed that the low frequency response of the amplifier is determined by only one RC circuit. In reality there is an RC coupling network between each of the amplifier stages. This results in an undershoot of the pulse as shown in the

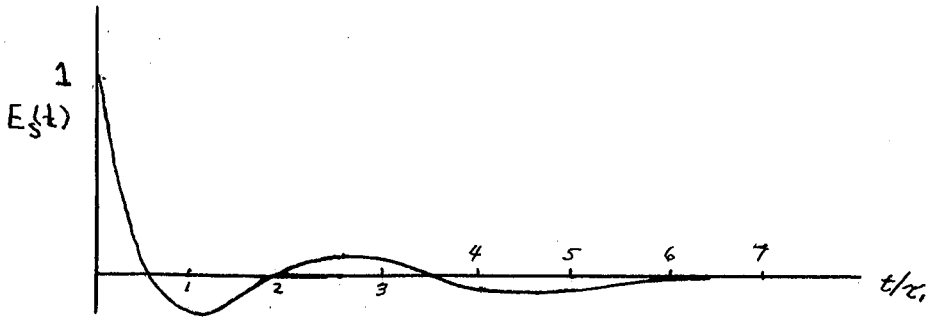

accompanying figure which applies to a step wave applied to a four stage amplifier where all the coupling time constants are equal. The solution of this problem is easily obtained. Consider a step wave applied to an n stage RC coupled amplifier with all the time constants equal to τ_1. The Laplace transform of the output is given by

$$\mathcal{L}[E_s(t)] = \frac{S^{n-1}}{\left(S + \frac{1}{\tau_1}\right)^n} \tag{28}$$

and the solution is

$$E_s(t) = (-1)^{n-1} e^{-t/\tau_1} L_{n-1}\left(\frac{t}{\tau_1}\right) \tag{29}$$

where $L_n(x)$ is the n^{th} Laguerre polynomial. These are the same as the radial wave functions of the hydrogen atom and Table (I) lists the amount of undershoot of E_o, the amount of the overshoot, and the time these occur.

TABLE I

Amplifier Overshoot

Stages	1st overshoot %	1st overshoot at t/τ	2nd overshoot %	2nd overshoot at t/τ
1	-8	3.0	0	-
2	-20	1.5	1.7	6.0
3	-24	1.0	4.0	4.0
4	-27	0.85	6.7	2.9
5	-29	0.7	9.5	2.3
6	-30	0.6	11.0	2.0
7	-31	0.5	12.5	1.8
8	-32	0.4	14.0	1.5
9	-33	0.4	15.0	1.3
10	-33	0.4	15.0	1.3

The undershoot is particularly bad, since if pulses are being counted which have a broad distribution of pulse heights, a small pulse occurring during the undershoot of the preceding pulse will not be counted. The overshoot is bad because at low bias settings of the discriminator one pulse may count twice. Elmore has estimated (Ref. 10) that if the differentiating time constant is less than 1% of the coupling time constant then the undershoot will be less than 1%. For a many stage amplifier Table (I) would seem to indicate that one should differentiate

even more rapidly than this. The undershoot of a rectangular pulse of duration τ_0 is easily calculated if $\tau_0 \ll \tau_1$. If the undershoot is E_u, then

$$E_u = -\tau_0 \left.\frac{dE_s}{dt}\right|_{t=0}$$

$$= (n-1)\left(\frac{\tau_0}{\tau_1}\right) \qquad \text{neglecting (higher order terms.)} \tag{30}$$

Thus for an undershoot of 1% with a 11 stage amplifier, one must differentiate with a time constant of $0.001\tau_1$. Since the amplifier is stabilized by feed-back, the low frequency response of the sections enclosed by the feed-back loops is very good but there are 3 coupling circuits between the feed-back units to which the above theory applies.

PART V

BIAS CURVES

Bias curves were obtained on protons of various energies and are shown in Fig. (10). An examination of these curves shows the length of the plateau is proportional to the particle energy. The sharp break in the curves at low bias values is due to the thermal noise from the tube. The long tail at high bias values is the result of the optical system having different efficiencies for different portions of the screen. The point just before the break in the plateau due to noise represents a counting efficiency of close to 100%. This was ascertained by comparisons with a ionization chamber and the ratio of scintillation counts to ion chamber counts is shown in Table II. It is also seen from the

TABLE II

Proton Energy Kev	Ratio
260	1.01
296	1.00
440	0.87
520	1.03
590	1.03
630	1.03
665	1.00
700	0.95

bias curves that all the protons may be counted down to an energy of 100 Kev below which noise seriously interferes with the plateau.

Bias curves for Li^6 ions, α-particles, deuterons and protons have been obtained. It was possible to obtain the proton and deuteron

curves under identical conditions, and the curves for the two cases were identical for particles having the same energy. Bias curves for α-particles and Li^6 ions seem to fall off somewhat faster than the corresponding curves for protons of the same energy indicating a smaller efficiency.

In an effort to determine the low energy limit of the usefulness of the detector, some low energy experiments were performed. The 931-A was sealed onto an accelerator whose voltage range was 15 - 100 Kev. The beam was very intense so that it was necessary to reduce its intensity by scattering the protons at an angle of 90° from a gold foil target which was thick compared to the proton energies used. The scattered protons then entered the detector which was cooled to dry ice temperatures. Proton energies of 17 Kev gave signals the maximum of which was some ten times greater than the background. The low energy limit was clearly not reached in this test, and the fact that 17 Kev protons gave a good signal is indicative of the high effeciency with which the phosphor converts the kinetic energy of the particle into light.

PART VI

CALIBRATION OF EQUIPMENT

Since the experiments were undertaken to establish accurately nuclear Q-values, the method of calibrating the equipment will be discussed. The 90° electrostatic analyzer previously described (1) was calibrated by measurements upon the γ-ray resonance in the $F^{19}(p,\alpha',\gamma)O^{16}$ reaction, which has been standardized at 873.5 Kev (11). The analyzer was then assumed to be linear with the voltage impressed upon its plates.

Once calibrated, the electrostatic analyzer furnished a means of calibrating the magnetic spectrograph. Protons and deuterons of known energy were elastically scattered from Be^9, C^{12}, O^{16} and copper. The energy of the protons leaving the surface of the targets and hence having the maximum energy can be easily calculated. These then furnish sufficient data to determine the constant C_m in Eq. (15) after the appropriate relativistic corrections have been made. A typical curve obtained by scattering protons of 948.5 Kev energy from a thick polished copper target is shown in Fig. (11). Since the window of the spectrograph is known to be symmetrical, the point of half maximum is taken as representing the energy of protons leaving the surface of the target at a mean angle of 79.9°.

Layers of C^{12} and O^{16} have been found on all the targets used by observing the protons elastically scattered from these layers in the high resolution magnetic spectrograph. The thickness of these layers is easily calculated since the number of protons scattered into the spectrograph is proportional to the number of atoms in the layer as long as the layer is thin compared to the spectrograph window, and the number scattered per atom may be estimated from Rutherford's formula.

These layers generally amounted to 0.45 Kev normal to the target for protons of energy 1.23 Mev. This standard layer was assumed in calculating C_m for the data obtained from the copper targets even though this could not be measured due to the fact that the protons scattered by copper obscure those scattered from oxygen due to their greater energy.

The angle was determined in two ways. First a direct measurement was made by admitting protons into the spectrograph through a slit system which accurately defined their angle, and observing the counts in the spectrograph as a function of this angle. Curves obtained at about 80° are shown in Fig. (2) with the entrance aperture of the spectrograph full open.* Not only the angle, but also the angular opening of the spectrograph may thus be obtained. Second, the energy of protons elastically scattered from various elements is a function of the angle θ and the mass M_o of the target nucleus. Thus we have

$$E_2^{1/2} = E_1^{1/2} k \tag{31}$$

$$k = \frac{M_1 \cos\theta}{M_1 + M_o} + \sqrt{\frac{M_o - M_1}{M_o + M_1} + \frac{M_1^2 \cos^2\theta}{(M_1 + M_o)^2}} \tag{32}$$

The value of C_m was calculated for Be^9, C^{12}, O^{16} and copper by using

---

* The actual data must be multiplied by $\sin^4\frac{\theta}{2}$ to remove the angular dependence of the elastic scattering cross section before a symmetrical curve is obtained.

the value of Θ obtained by direct measurement. If the value for the angle were wrong the value of C_m obtained from Be^9 would differ from that for copper since beryllium is so light. Table (III) shows a sequence of measurements of C_m, and the consistency of the values indicates that the angle was accurately known.

The probable systematic errors were taken to be as follows: bombarding energy 0.2%, observed energy in spectrograph 0.3% and angle of observation 0.3°. These errors were combined with the observed statistical errors in the following calculations to give the total errors.

TABLE III

Table of Spectrograph Constant at $\Theta = 80^\circ$

Bombarding Energy	Target	$C_m \times 10^{-6}$
948.5	Be^9	1.699
	Be^9	1.710
	C^{12}	1.711
	C^{12}	1.730
	O^{16}	1.710
	Cu	1.719
	Cu	1.727
603.3	Be^9	1.712
	Be^9	1.709
	C^{12}	1.721
	O^{16}	1.722
	O^{16}	1.716
	Cu	1.725

Average C_m (1.716 0.002) X 10^6

PART VII

RESULTS

The $Be^9(p,\alpha)Li^6$ and $Be^9(p,d)$ Reactions

The reactions (1), (2) and (3) were investigated using thin beryllium foil targets. Fig. (12) and Fig. (13) show the curves obtained at proton energies of 603 Kev and 949 Kev respectively. The angle of observation was 80° and the beryllium foil was 15 Kev thick for 1 Mev protons.* In Fig. (12) the peak at ~ 60 mv is due to elastically scattered protons from the beryllium foil whose normal was set at an angle of 60° with respect to the beam direction. The width of this peak can be used to calculate the thickness of the target. The two small peaks at 57 and 58 mv are the peaks due to O^{16} and C^{12} respectively. Very thin layers of carbon and oxygen were found on all the beryllium and lithium targets used. The layers are thinner than the resolution of the spectrograph and their width is a measure of this factor. In this case the height of the peak can be used as previously explained to calculate the carbon and oxygen layer thickness which was found to be 0.45 Kev measured normal to the target.

The peak located at 33 mv represents the α particles from the $Be^9(p,\alpha)Li^6$ reaction. They are superimposed upon the doubly ionized Li^6 ions from the same reaction. The α particles have an energy of ~ 1.6 Mev whereas the Li^6 ions have nearly the same momentum but an energy of only ~ 1 Mev. These two ions were separated by placing thin aluminum foils directly in front of the ZnS screen of the detector. The Li^6 ions were stopped and the α particles counted and the difference between this number and the number of counts with no foil was used to obtain the

---

* This refers to the actual foil thickness. The effective thickness depends upon the orientation of the foil with respect to the beam direction.

number of Li^6 ions alone. Since the stopping power of matter is higher for Li^6 ions than for α particles the target appears thicker for them. The triply ionized Li^6 ions from this same reaction appear at 50 mv. The single charged Li^6 and He^4 ions from this reaction could not be observed in the spectrograph due to the large field that would be necessary to deflect them.

The deuterons from the reaction $Be^9(p,d)Be^8$ appear as a sharp peak at 32 mv. The fact that all the deuterons have the same energy indicates that Be^8 is formed and has a half life long enough to give two body dynamics to the reaction. The deuteron energy and the bombarding energy furnish data to uniquely determine the Q of this reaction. The Be^8 ions were looked for and not found. However, the spectrum beginning at 57 mv and extending back was identified as the singly charged α-particles resulting from the break up of the recoiling Be^8 nucleus. The doubly ionized Li^6 peak gave some interference with this spectrum, and here again a foil in front of the multiplier thick enough to stop the low energy α-particles and thin enough to pass the high energy Li^6 ions served to separate the two particle groups.

The Be^8 residual nucleus recoils after emission of the deuteron and has so short a life time that it decays before stopping. The stopping time is of the order of 10^{-13} seconds which is much longer than the estimated life time of Be^8 in the ground state. Since the Be^8 is in motion when it decays, the resulting α-particles will have a continuous spectrum. Assuming isotropy in both the primary and secondary reaction the differential spectrum may be calculated in the laboratory system and is for the cases studied:

$$N(E_\alpha)\, dE_\alpha\, d\Omega = \frac{N_0 E_\alpha^{1/2}\, dE_\alpha\, d\Omega}{\sqrt{E_\alpha + C_1 E_p - 2\sqrt{C_2 E_\alpha E_p}\cos\theta}}$$

$$C_1 = \frac{M_{H^1} M_{He^4}}{(M_{H^1} + M_{Be^9})^2} = 0.04 \qquad (33)$$

$$C_2 = \frac{M_{He^4}}{M_{H^1} + M_{Be^9}} = 0.4$$

where E_α is the observed α particle energy, E_p is the bombarding proton energy, and θ is the angle of observation. This differential spectrum is shown plotted in Fig. (14) for $E_p = 940$ Kev, $\theta = 80^\circ$. The beryllium foil target actually used was more than 100 Kev thick for these low energy α particles and hence this differential spectrum will be integrated over this thickness of target. It is apparent that in the first approximation this will lead to a straight line sloping up from the maximum of the α particle energy. Deviations should only become apparent 100 Kev or more from the end point. Fig. (15) shows the α spectrum of Fig. (12) converted to an energy plot and the linear character of the spectrum is evident. The "fillet" near the end point is just accounted for by instrument resolution. A similar plot was made for the data at 949 Kev and the end point obtained in this case also. The two sets of data give 89.0 and 89.4 Kev respectively for the Q value of the $Be^8(\alpha)He^4$ reaction.

The data taken to determine the $Be^9(p,\alpha)Li^6$ and $Be^9(p,d)Be^8$ Q values are summarized in Table (IV). The averaged values for these

are $Q_1 = 2.121 \pm 0.012$ Mev, $Q_2 = 0.558 \pm 0.003$ Mev, and $Q_3 = 0.089 \pm 0.005$ Mev.

TABLE IV

$Be^9(p,\alpha)Li^6$

E_p	Particle Observed	Θ	Q (Mev)
495	α	137.8°	2.101
	Li^{++} / Li^{+++}	80.0°	2.120
605	α	80.0°	2.121
741	α	137.8°	2.128
952	α	80.0°	2.110
989	α	137.8°	2.128
1.113	α	137.8°	2.154
	Weighted Average		2.121

$Be^9(p,d)Be^8$

495	d	137.8°	.555
605	d	80.0°	.555
741	d	137.8°	.566
989	d	137.8°	.555
1.113	d	137.8°	.561
	Weighted Average		.558

$Li^6(p,\alpha)He^3$

In this case thin lithium targets were evaporated in vacua onto a copper support. A typical curve obtained is shown in the insert of Fig. 12. The angle of observation in this case was 137.8° and the bombarding energy 742 Kev. The two peaks at 33.2 and 35 mv are He^3 and He^4 doubly ionized particles respectively. The targets were made just thin enough to resolve these two peaks. The target appears thicker for the He^4 due to its lower velocity. The Q for the reaction was calculated from the He^4 and also He^3 data and is summarized in Table (V). The average value for the Q is 4.017 ± 0.022 Mev.

TABLE V

$Li^6(p,\alpha)He^3$

E_p	Particle Observed	θ	Q (Mev)
742	He^3	137.8°	4018
	He^4	137.8°	4014
1237	He^3	137.8°	4018
	He^4	137.8°	4017
		Average	4017

The $D(d,p)H^3$ and $D(d,n)He^3$ Reactions

Reactions (4) and (5) were primarily studied in order to obtain an accurate value for the neutron-atomic hydrogen mass difference as given by Eq. (8). This determination assumes that the mass of the neutrino is negligible since the (H^3 - He^3) mass difference is obtained from the end point of the β decay of H^3. It is shown in Ref. (4) that the shape of the β spectrum indicates that the neutrino mass is less than 1 Kev and hence is negligible.

The target was prepared by inserting into the target chamber of the spectrograph one end of a 1/2" copper rod about 12" long. The rod was insulated both thermally and electrically from the rest of the system by means of a glass to metal seal. The one end of the rod was placed in a container of liquid air, and heavy water vapor was admitted into the target chamber adjacent to the rod. The D_2O vapor condensed continuously on the rod thus insuring a clean target surface at all times. Oil vapors were trapped out of the system by liquid air traps located at the diffusion pumps. The target normal made an angle of 150° with respect to the beam and the angle of observation was 137.8°.

A Geiger Counter placed next to the target chamber was used to monitor the neutron yield from the $D(d,n)He^3$ reaction. The efficiency of the counter was very low of course, but the yield of the reaction is large enough to compensate for this factor. About 10% of the counts registered were from a γ-ray reaction produced in the oxygen by deuterons which was ascertained by replacing the heavy water with ordinary water. The thick target yield curve obtained with this counter was used to determine the target thickness when thin targets were used.

Fig. 16 shows a typical set of data obtained at a bombarding energy of 249 Kev. The target in this case was about 30 Kev thick for the deuterons and should therefore appear about 70 Kev thick for H^3. Thus the He^3 curve has the correct shape, but the H^3 peak has a half width which is almost completely accounted for by the resolution of the spectrograph due to the 6.6° entrance aperature employed here. This effect is a result of observing the reaction in the backward direction.

The recoil velocity of the compound nucleus in the forward direction reduces the energy of the H^3 particle observed in the backward direction. Thus the less the bombarding energy, the greater will be the observed energy of the H^3 particles. Therefore the H^3 particles formed at the surface of the target will have less energy than those formed deep in the target which however must lose energy in order to escape the target. The total effect of stopping power and change of energy of the emitted particle with the energy of the incident deuteron can be calculated and is compiled in Table (VI), where ξ is the target thickness for the deuterons and E_2 is the energy spread observed for the H^3 particles.

TABLE VI

Bombarding Energy (Kev)	H^3 Energy (Kev)	E_2/ξ
248	603	0.139
311	555	0.258
448	481	0.457
498	456	0.533
623	396	0.71

Thus for the curve shown in Fig. 16 where the target thickness was ~ 30

Kev a spread in the energy of the H^3 should be 30 X 0.139 or approximately 4 Kev which combined with the window due to the entrance angular opening of 27 Kev explains the width of the observed peak. This effect is not observed for the He^3 due to the much greater stopping power of the target for these particles. The "fillet" at the foot of the high energy side of the H^3 peak is due to the crystalline nature of the target which enables some of the H^3 formed in the target to escape without traversing the total thickness of the target and thus to appear with more energy than those formed at the surface.

Thick, semi-thick, and thin targets were used and consequently a careful analysis of the effect of the various window curves of the spectrograph was made. The variation with entrance angle of the opening of the spectrograph is shown in Fig. 2 and is very closely represented by a parabola. It can be converted into an energy window by differentiating the following equation for E_2:

$$E_2^{1/2} = \left[\frac{M_1 M_2 E_1 \cos^2\theta}{M^2}\right]^{1/2} + \sqrt{\frac{M-M_2}{M} Q + \frac{M-M_2-M_1}{M} E_1 + \frac{M_1 M_2 E_1 \cos^2\theta}{M^2}} \qquad (34)$$

$$\frac{1}{E_2^{1/2}} \frac{\partial E_2}{\partial \theta} = 2\sqrt{\frac{M_1 M_2 E_1}{M^2}} \sin^2\theta + \frac{M_1 M_2 E_1 \sin 2\theta}{M^2 \sqrt{\frac{M-M_2}{M} Q + \frac{M-M_2-M_1}{M} E_1 + \frac{M_1 M_2 E_1 \cos^2\theta}{M^2}}} \qquad (35)$$

where M_1 is the mass of the bombarding particle and E_1 its energy, M_2 is the mass of the observed particle and E_2 its energy, M is the mass of the compound nucleus, and θ is the angle of observation. An

additional window is due to the finite size of the beam spot and the entrance hole to the scintillation counter. This is approximately given by a square window of half width $\Delta I_R = 0.0078I$ where I is the spectrograph current in millivolts and is about 1/4 the width of the window due to the angular opening. The target was represented by a square window whose width was obtained by multiplying the true target thickness as obtained from the neutron yield curve by the factor given in Table (VI). Straggling was negligible for all cases considered.

Thick targets were treated by recording the extrapolated end point and the mid-point for each separate run. By folding the above two windows into a thick target curve it is found that the relation between the mid-point and the extrapolated end point is given by

$$I_{1/2} = I_x + \tfrac{2}{3}\,\Delta I_\theta \left[1 + \tfrac{1}{3} \left(\frac{\Delta I_R}{\Delta I_\theta} \right)^2 \right] \qquad (36)$$

where $I_{1/2}$ is the mid-point, I_x the extrapolated end point and ΔI_θ is the half width of the window due to the angular opening and is calculated by Eq. (35). The observed and calculated mid-points were found to agree very well in this case.

Target thicknesses comparable to ΔI_θ were considered semi-thick targets. In this case the peak of the curve and the extrapolated front edge were measured. Theoretical curves were then calculated for the various semi-thick targets used. These curves were then measured to obtain the correction necessary to convert the reading for the peak and the extrapolated end point to the equivalent mid-point value for a thick target. Since the number of counts on the flat part of the

thick target curve is known, and the target thickness is known from the yield curve measurement, it should be possible by folding the above windows into each other to also calculate the number of counts obtained at the peak of a semi-thick target curve. It was possible to calculate this number to within about 5% of the actual number observed.

Thin targets arise when the target thickness is small compared to ΔI_θ. The extrapolated end points and the peaks were measured and calculations show that

$$I_{1/2} = I_{MAX} - \Delta I_T \tag{37}$$

and also that

$$I_{1/2} = I_x + \Delta I_\theta \left\{ 1 + 1/3 \left(\frac{\Delta I_R}{\Delta I_\theta} \right)^2 \right\} - \Delta I_T \tag{38}$$

where $I_{1/2}$ is the magnetometer reading which corresponds to particles from the front surface of the target entering the center of the spectrograph window, ΔI_T the equivalent half target thickness computed from 1/2 the actual target thickness times the factor given in Table (VI).

Table (VII) gives the results of this analysis at various bombarding energies and target thicknesses. The last column gives the final value for $I_{1/2}$ adopted in each case and the weight assigned to the measurement. The mid-points of the He^3 curves were used in each case, as they all corresponded to a thick target curve. The results of the Q calculations are summarized in Table (VIII) and the weighted averages are $Q_5 = 4.036 \pm 0.022$ Mev and $Q_4 = 3.265 \pm 0.018$ Mev which when combined with the weighted average of Ref. (5) and (6) for

TABLE VII

Thick Target

	Measured						Calculated			
Deuteron Energy	I_X	$I_{1/2}$	I_{max}	ΔI_e	ΔI_R	ΔI_T	$I_{1/2}$	$I_{1/2}$ Adopted		Weight
623	37.50	37.94	38.80	0.72	0.15	very thick	37.98	37.96		2
498	35.08	35.46	36.40	0.60	0.14	0.67	35.48	35.54		2
	35.12	35.69	36.60	0.60	0.14	0.55	35.52			
				Semi Thick Targets						
448	34.32	-	-	0.54	0.14	0.20	34.82			
	34.30	-	-	0.54	0.14	0.35	34.69	34.73		3
	34.19	-	-	0.54	0.14	0.55	34.58			
							Calculated			
				Thin Targets			I_{max}	$I_{1/2}$		
311	31.89		32.38	0.42	0.13	0.115	32.38	32.37	32.27	2
248	30.74		31.16	0.36	0.13	0.01	32.12	31.11		3
	30.70		31.15	0.36	0.13	0.005	31.08	31.07	31.09	
	30.65		31.08	0.36	0.13	0.050	31.07	31.02		
	30.69		31.08	0.36	0.13	0.036	31.11	31.07	31.05	1

$(H^3 - He^3) = 0.0183 \pm 0.0003$ Mev yields $n^1 - H^1 = 0.789 \pm 0.005$ Mev. The error in $n^1 - H^1$ depends upon $Q_5 - Q_4$ and since in all cases the data were obtained by making observations on both the H^3 and He^3 in succession as rapidly as possible the error in $n^1 - H^1$ depends mainly upon the error $I_{He^3} - I_{H^3}$ and was not computed from the errors in Q_5 and Q_4 taken as independent observations.

TABLE VIII

Bombarding Energy (Kev)	Energy H^{3+} (Kev)	Energy He^{3+} (Kev)	Q_5 (Kev)	Q_4 (Kev)	Weight
247.1	599.4	455.2	4028	3271	3
248.9	600.8	455.4	4041	3279	1
311.2	556.2	414.6	4031	3259	2
448.3	480.2	348.1	4039	3259	3
498.2	458.6	329.0	4053	3268	2
622.7	401.9	--	4032	--	2
* 164.6	--	514.4	--	3264	1

* Measurement on He^{3++} curve.

$B^{10}(p,\alpha)Be^{7}$ Reaction

Boric acid containing B^{10} isotope was evaporated in vacua onto a copper support. The water is apparently given off at a few hundred degrees centigrade and the target material was undoubtedly $B_2^{10}O_3$ which evaporated at a bright white heat. Five runs were made with a new target each time at three different voltages and in each case at an angle of observation of 137.8°. The target was pure enough so that there was negligible interference from the $B^{11}(p,\alpha)$ reactions. The final average value for the Q is 1.146 ± 0.005 Mev.

DISCUSSION OF RESULTS

The results of this investigation are tabulated for convenience in the following table.

TABLE IX

Reaction	Q (Mev)
$Be^9(p,\alpha)Li^6$	$Q_1 = 2.121 \pm 0.012$
$Be^9(p,d)Be^8$	$Q_2 = 0.558 \pm 0.003$
$Be^8(\alpha)He^4$	$Q_3 = 0.089 \pm 0.005$
$D(d,n)He^3$	$Q_4 = 3.265 \pm 0.018$
$D(d,p)H^3$	$Q_5 = 4.036 \pm 0.022$
$Li^6(p,\alpha)He^3$	$Q_6 = 4.017 \pm 0.022$
$B^{10}(p,\alpha)Be^7$	$Q_7 = 1.146 \pm 0.005$
$(n^1 - H^1)$	$= 0.789 \pm 0.005$

Q_1 and Q_2 are both somewhat higher than the earlier measurements of Rosario [12] and of Perlow [13]. Q_3 is to be compared to 102 ± 10 Kev obtained by Hemmindinger after his results are corrected for γ-ray recoil [4]. Q_2 may be combined with the most recent value for the binding energy of the deuteron obtained by Bell and Elliott [14] of 2.230 ± 0.007 Mev to give

$$Be^9 + \gamma = n + Be^8 + Q_8 \qquad (39)$$

where Q_8 is found to be -1.672 ± 0.008 Mev. The ratio of this Q to that for $H^2(n,\gamma)H^1$ is -1.334 ± 0.010 which is in excellent agreement with -1.338 ± 0.004 found by Waldman and Miller [15].

The value of Q_5 is considerably higher than the previously accepted value of 3.98 Mev [16]. The $n^1 - H^1$ difference determined

here is in fair agreement with the value of 782 ± 2 Kev [17] and 776 ± 10 [18] which were determined from (p,n) reaction thresholds.

The two reactions (6) and (7) both determine points on the range energy curve. We have from (4), (5) and (6)

$$Li^6 + n = He^4 + H^3 + 4.788 \pm 0.023 \text{ Mev} \qquad (40)$$

and from (7) combined with the accurately determined Q for Li^7 (p,n)Be^7 of 1.646 ± 0.002 Mev it is found that

$$B^{10} + n = Li^7 + He^4 + 2.792 \pm 0.006 \text{ Mev.} \qquad (41)$$

Approximately 85% of the time this latter reaction leaves the Li^7 residual nucleus in its first excited state at 0.477 ± 0.001 Kev Ref. (19). Thus one has

$$B^{10} + n = Li^{7*} + He^4 + 2.315 \pm 0.006 \text{ Mev.} \qquad (42)$$

A re-examination of the range energy relations has been made by Bethe on the basis of these and other reactions, so no attempt will be made here to assign ranges to the above particles.

A complete summary of all the accurately known Q-values is included in the following reprint.

REFERENCES

1. Fowler, Lauritsen, and Lauritsen, Rev. Sci. Inst. 18, 818 (1947).

2. Snyder, Lauritsen, Fowler and Rubin, Phys. Rev. 74, 1564(A) (1948).

3. Wheeler, Phys. Rev. 59, 27 (1941).

4. A. Hemmendinger, Phys. Rev. 73, 806 (1948); Phys. Rev. 74, 1267 (1948).

5. S. C. Curran, J. Angus, A. L. Cockroft, Phil. Mag. 40, 53 (1949).

6. G. E. Hanna and B. Ponticorvo, Phys. Rev. 75, 983 (1949).

7. C. C. Lauritsen and T. Lauritsen, Rev. Sci. Inst. 19, 916 (1948).

8. Coltman and Marshall, Nucleonics Vol I, No 3, Page 58 (1947).

9. R. W. Engstrom, Journal Optical Soc. 37, 420 (1947).

10. Experimental Electronics, Elmore and Sands, McGraw - Hill (1950).

11. Herb Snowdon, Sala, Phys. Rev. 75, 246 (1949).

12. Leitcio del Rosario, Phys. Rev. 74, 304 (1948).

13. G. J. Perlow, Phys. Rev. 58, 218 (1940).

14. Private Communication.

15. B. Waldman and W. C. Miller, Phys. Rev. 74, 1225(A) (1948).

16. Oliphant, Kempton and Rutherford, Proc. Roy. Soc. 144, 692 (1934).
M. S. Livingston and H. A. Bethe, Rev. Mod. Phys. 9, 245 (1937).

17. Taschek, Argo, Hemmendinger and Jarvis, Phys. Rev. 76, 325 (1949).

18. W. E. Shoupp, B. Jennings and K. H. Sun, Phys. Rev. 75, 1 (1949).

19. W. A. Fowler, C. C. Lauritsen and S. Rubin, Phys. Rev. 75, 1471(A) (1949).

NUCLEAR MASS DETERMINATION FROM NUCLEAR Q-VALUES

A. Tollestrup, W. A. Fowler and C. C. Lauritsen

Kellogg Radiation Laboratory, California Institute of Technology

Pasadena 4, California

Physical Review 78, 372 (1950)

The Q-values for several reactions involving light nuclei have been recently measured with probable errors of 20 kev or less. In general these measurements have been made possible through the employment of high resolution electrostatic or magnetic analysers for determining the energy of the particles involved in the reaction. These new data are sufficient to determine the nuclear masses relative to H^1 through B^{10}, independently of mass spectroscopic data. Unfortunately sufficient data are not yet available to base the masses upon O^{16} and consequently the mass spectroscopic value for H^1 is used. Furthermore some uncertainty still exists in the mass of He^4 and subsequent nuclei as discussed below.

The mass values of H^1, D^2, C^{12} and N^{14} were calculated from the mass spectroscopic doublets 2H-D, CH^4-O, CH^2-N^{14}, and $3D$-$C_{1/2}$ and are given in column 1 of Table II. In view of the discrepancies recently found in the early values of 2H-D, it was decided to use Nier's[1] recent values for the first three doublets combined with the results of Bainbridge[2] for the last doublet.* Nier's value for 2H-D combined with Bell and Elliott's[3] new value for $H^1(n\gamma)D$ leads

---

* It is emphasized that a future change in the mass spectroscopic value of H^1 will change the masses for D^2 to B^{10} inclusive by the same amount.

to an n-H^1 difference of 788 kev compared to 782 ± 1 kev as determined at Los Alamos from threshold measurements on $T^3(p,n)He^3$ combined with the decay energy of tritium. The nuclear data have been combined with the mass spectroscopic values of C^{12} and N^{14} to yield the masses of N^{13}, C^{13}, and C^{14}.

Table 1 lists all the accurately determined Q-values considered in this note. The $Li^7(p,\alpha)He^4$ value is not new but was included in order to determine the mass of the α particle and hence it influences all subsequent masses. The range of the α particles from this reaction nearly coincides with the range of those from ThC' and hence the measurement was considered more accurate than that of $Li^6(d,\alpha)He^4$ which if accurately known could also be used to determine the α particle mass.

Among the data listed, there are eight independent cycles which determine the n-H^1 difference, the values ranging from 776 ± 9 to 789 ± 6 kev. The weighted mean of 782 ± 1 kev is almost entirely determined by the Los Alamos data. Using this value the Q-values in each case were adjusted to be consistent with this difference. The adjustments made were weighted according to the experimental errors given and in no case did the change exceed 7 kev with the single exception of Townsend's value for $C^{11}(\beta^+)B^{11}$. Since the value of the $B^{11}(p,n)C^{11}$ threshold is very accurately known, the whole discrepancy of 23 kev in this case was ascribed to the $C^{11}(\beta^+)B^{11}$ determination. It was found that Townsend's measurement of $N^{13}(\beta^+)C^{13}$ was also some 20 kev different from two other precise measurements which agreed with each other. (See NRC Nuclear Science Series #5) Consequently we have not included his results in adjusting the Q-values.

Finally all other independent cycles among the reactions listed were considered. There are seven of these, and the Q-values in each case were adjusted in relation to the experimental errors to satisfy the cycles; in no case did this adjustment require a change of more than 9 Kev, nor were any of the experimental errors exceeded. These adopted Q-values are listed in column 3 of Table I together with the reference. The values are given in Mev and in milli-mass units based upon 1 mmu = 0.9311 Mev. These Q-values were then combined with the mass spectroscopic value for H^1 to yield the masses which are listed in Table II, while the mass spectroscopic data for C^{12}, N^{14} were also used to yield the masses of N^{13}, C^{13}, C^{14}. For comparison the values given in "Elementary Nuclear Physics" by H. A. Bethe are also listed together with the differences.

It is evident from the above that the reactions $Li^6(d,\alpha)$ and $Li^7(p,\alpha)$ should be accurately determined in a high resolution spectrograph in order to fix the α particle mass. This would make the nuclear data satisfactory up to B^{10}. The H^1, D^2, C^{12}, O^{16} system is one of the basic mass spectroscopic cycles, and should be checked by nuclear methods. As mentioned earlier, the H^1 to D^2 part of this cycle now agrees with nuclear data, and the remaining two intervals D^2 to C^{12} and C^{12} to O^{16} offer two remaining checks on these data. C^{12} can be obtained from existing data if the two reactions, $B^{10}(d,p)B^{11}$ ($Q \sim 9$ Mev) and $C^{13}(d,\alpha)B^{11}$ ($Q \sim 5$ Mev), are determined accurately. Furthermore, the series $O^{16}(d,\alpha)N^{14}$ ($Q \sim 3$ Mev), $N^{14}(n,\alpha)B^{11}$ ($Q \sim -0.3$ Mev) and $B^{10}(d,p)B^{11}$ would connect B^{10} directly with O^{16}, but has the disadvantage of involving a neutron induced reaction with a negative Q. While the

internal consistency of the nuclear data seems very good, a compounding of errors is certainly possible and comparisons with the mass spectroscopic values are very desirable.

REFERENCES

(1) Bull APS, Vol. 24, #7, page 20.

(2) NRC Nuclear Science Series #1.

(3) Private Communication from R. E. Bell and R. G. Elliott.

TABLE I

Table of Accurate Q-Values

Reaction	Q-Measured	Adopted Q* Mev	Adopted Q* mmu	Reference
$H^1(n,\gamma)D^2$	2.230 ± 0.007	2.230	2.395	Bell & Elliott, Priv. Comm.
$D^2(\gamma,n)H^1$	-2.186 ± 0.004	-2.230	-2.395	NRC Nuclear Science Series #1
$D^2(d,p)T^3$	4.036 ± 0.022	4.032	4.330	Phys. Rev. 75, 1947 (1949)
$D^2(d,n)He^3$	3.265 ± 0.018	3.268	3.510	Phys. Rev. 75, 1947 (1949)
$T^3(\beta)He^3$	0.0189 ± 0.0005 0.0180 to 0.0186	0.0185	0.0199	Phys. Rev. 75, 984 (1949) Phys. Rev. 76, 853 (1949)
$T^3(p,n)He^3$	-0.7637 ± 0.001	-0.7637	-0.8202	Phys. Rev. 76, 325 (1949)
$He^3(n,p)T^3$	0.764 ± 0.010 0.766 ± 0.010	0.7637	0.8202	Phys. Rev. 75, 1110 (1949) W. Franzen, et al, Priv. Comm.
$Li^6(n,\alpha)T^3$	4.56 ± .08** 4.92 ± .03**	4.785	5.139	Phys. Rev. 75, 782 (1949) Phys. Rev. 75, 782 (1949)
$Li^6(p,\alpha)He^3$	4.017 ± 0.022	4.021	4.319	Phys. Rev. 76, 428 (1949)
$Li^6(d,p)Li^7$	5.006 ± 0.016	5.012	5.383	Phys. Rev. 76, 1766 (1949)
$Li^6(d,\alpha)He^4$	22.20 ± 0.04	(22.292)	(23.942)	Phys. Rev. 56, 548 (1949)

* 1 mmu 0.9311 Mev.

** When corrected for the new Range Energy relation Phys. Rev. 75, 1110, (1949) these results are close to the adopted value

Table I (cont.)

Reaction	Q-Measured	Adopted Q* Mev	Adopted Q* mmu	Reference
$Li^7(d,p)Li^8$	-0.193	-0.193	-0.207	Phys. Rev. 76, 1766 (1949)
$Li^7(p,\alpha)He^4$	17.28 ± 0.03	17.280	18.559	Phys. Rev. 56, 548 (1949)
$Li^7(p,n)Be^7$	1.6456 ± 0.00016 1.6449	-1.6453	-1.767	Phys. Rev. 75, 246 (1949) Phys. Rev. 76, 502 (1949)
$Be^8(\alpha)He^4$	0.089 ± 0.005	0.089	-0.0956	Phys. Rev. 76, 428 (1949)
$Be^9(\gamma,n)Be^8$	$-\frac{2.230}{1.338} = -1.667$	-1.671	-1.795	Phys. Rev. 74, 1225(A) (1949)
$Be^9(p,n)\ B^9$	1.851 ± 0.006 1.8519 ± 0.002	-1.8514	-1.9884	Phys. Rev. 65, 33 (1944) Bull APS Vol. 24, #7 page 20
$Be^9(p,d)Be^8$	0.558 ± 0.003	0.559	0.600	Phys. Rev. 76, 428 (1949)
$Be^9(p,\alpha)Li^6$	2.121 ± 0.012	2.125	2.282	Phys. Rev. 76, 428 (1949)
$Be^9(d,p)Be^{10}$	4.576 ± 0.012	4.568	4.906	Phys. Rev. 76, 1547 (1949)
$Be^9(d,\alpha)Li^7$	7.145 ± 0.024	7.137	7.665	Phys. Rev. 76, 1547 (1949)
$Be^{10}(\beta)B^{10}$	0.566 ± 0.010	0.560	0.601	Phys. Rev. 76, 183A (1949)
$B^{10}(p,\alpha)Be^7$	1.146 ± 0.005	1.146	1.231	Phys. Rev. 76, 587A (1949)
$B^{10}(n,\alpha)Li^7$	2.785 ± 0.025	2.791	2.998	Phys. Rev. 74, 1259(A) (1949)
$B^{11}(p,n)C^{11}$	-2.762 ± 0.002	-2.762	-2.966	Bull APS Vol 24, #7, page 20
$C^{11}(\beta^+)B^{11}$	2.003 ± 0.005	1.980	2.127	Proc. Roy. Soc. A177, 357 (1940-1941)

Table I (cont.)

Reaction	Q-Measured	Adopted Q* Mev	mmu	Reference
$C^{12}(d,p)C^{13}$	2.729 ± 0.009	2.726	2.928	Phys. Rev. 76, 1543 (1949)
$C^{12}(d,n)N^{13}$	-0.281 ± 0.003	-0.279	-0.300	Phys. Rev. 75, 1398 (1949)
$C^{13}(p,n)N^{13}$	-3.003 ± 0.003	-3.005	-3.227	Bull APS Vol 24, #7, page 20
$C^{14}(p,n)N^{14}$	-0.620 ± 0.009	-0.626	-0.672	Phys. Rev. 75, 1 (1949)
$C^{14}(\beta)N^{14}$	0.156 ± 0.001	0.156	0.168	NRC Nuclear Science Series #5
$N^{13}(\beta^{+})C^{13}$	2.222 ± 0.003	2.223	2.387	NRC Nuclear Science Series #5
$N^{14}(n,p)C^{14}$	0.616 ± 0.010			Phys. Rev. 75, 1110 (1949)
	0.630 ± 0.006	0.626	0.672	
$O^{16}(d,p)O^{17}$	1.925 ± 0.009	1.925	2.067	Phys. Rev. 76, 1543 (1949)
$O^{18}(p,n)F^{18}$	-2.455 ± 0.002	-2.455	-2.637	Bull APS Vol 24, #7, page 20
$F^{19}(p,\alpha)O^{16}$	8.113 ± 0.030	8.113	8.713	Bull APS Vol 24, #8, page 11

TABLE II

Table of Atomic Masses

	From Mass Spectroscopic Data	From Nuclear Data	Bethe	(mmu)
n^1		1. 008 977	1. 008 930	0.047
H^1	1. 008 137 4	*	1. 008 123	0.014
D^2	2. 014 726	2. 014 719	2. 014 708	0.011
T^3		3. 016 971	3. 017 02	- 0.05
He^3		3. 016 951	3. 017 00	- 0.05
He^4		4. 003 910	4. 003 90	0.01
Li^6		6. 017 043	6. 016 97	0.07
Li^7		7. 018 242	7. 018 22	0.02
Li^8		8. 025 031	8. 025 02	0.01
Be^7		7. 019 169	7. 019 16	0.01
Be^8		8. 007 916	8. 007 85	0.06
Be^9		9. 015 098	9. 015 03	0.07
Be^{10}		10. 016 774	10. 016 77	0
B^9		9. 016 246	9. 016 20	0.05
B^{10}		10. 016 173	10. 016 18	-0.01
C^{12}	12. 003 900	*	12. 003 82	0.08
C^{13}		13. 007 554	13. 007 51	0.04
C^{14}		14. 007 733	14. 007 67	0.06
N^{13}		13. 009 941	13. 009 88	- 0.04
N^{14}	14. 007 565	*	14. 007 51	0.05
O^{17}		17. 004 515	17. 004 50	0.02
F^{19}		19. 004 486	19. 004 50	- 0.01

* Mass spectroscopic values used here.

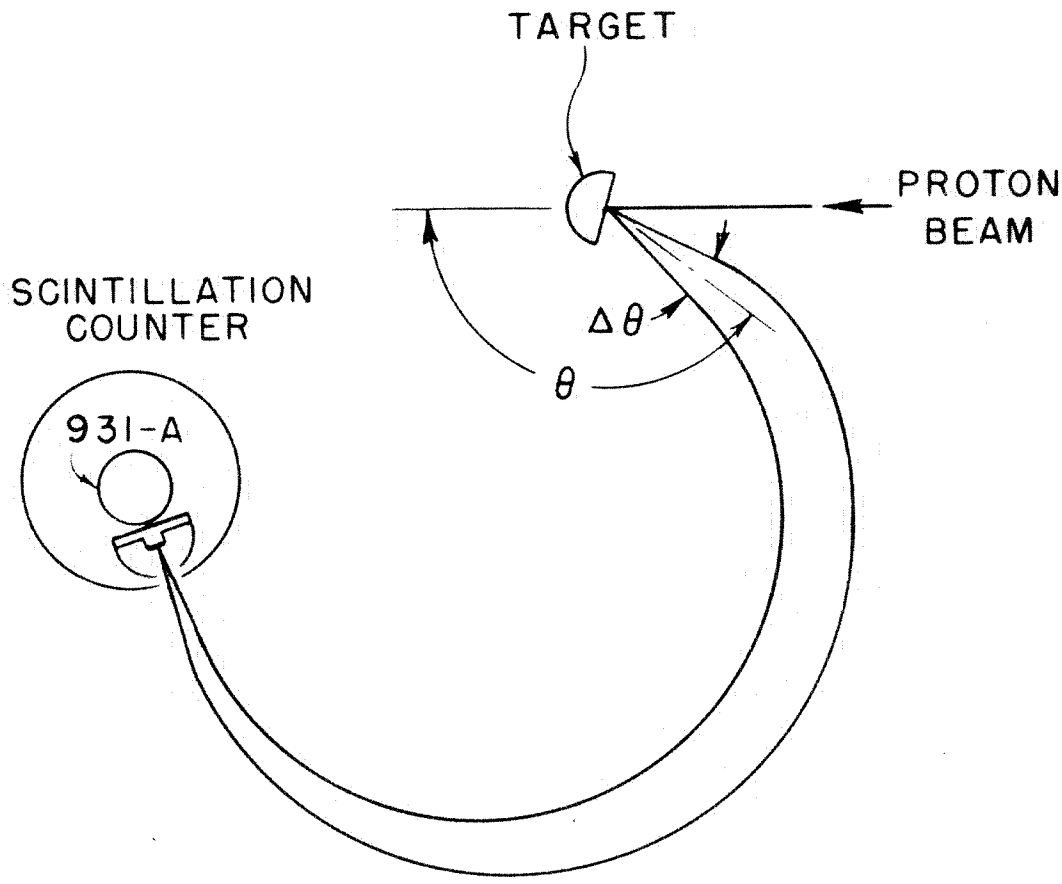

ARRANGEMENT OF EQUIPMENT

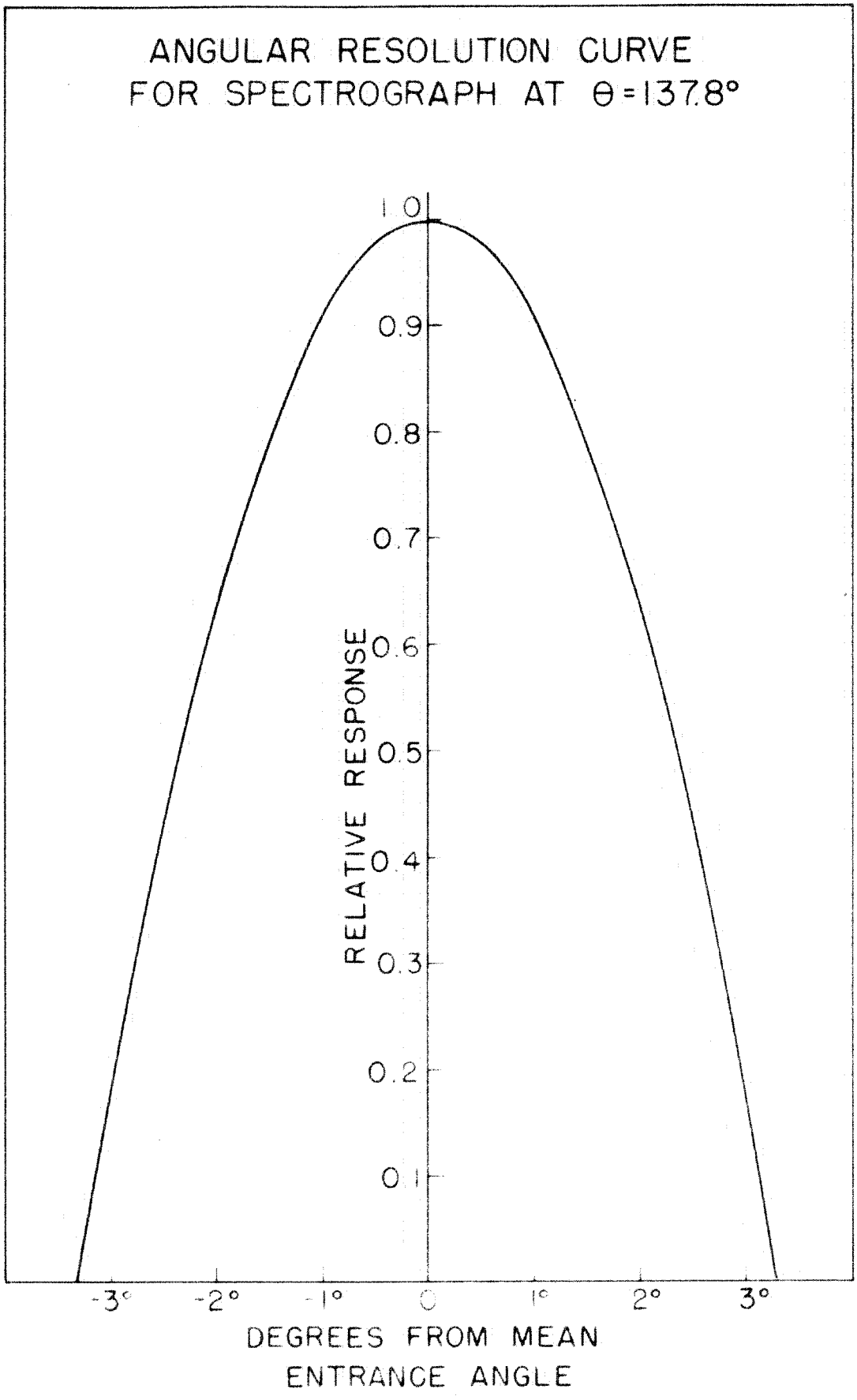
ANGULAR RESOLUTION CURVE
FOR SPECTROGRAPH AT θ=137.8°
1.0
0.9
0.8
0.7
0.6
0.5
0.4
0.3
0.2
0.1
RELATIVE RESPONSE
-3°
-2°
-1°
0
1°
2°
3°
DEGREES FROM MEAN
ENTRANCE ANGLE

Fig 3

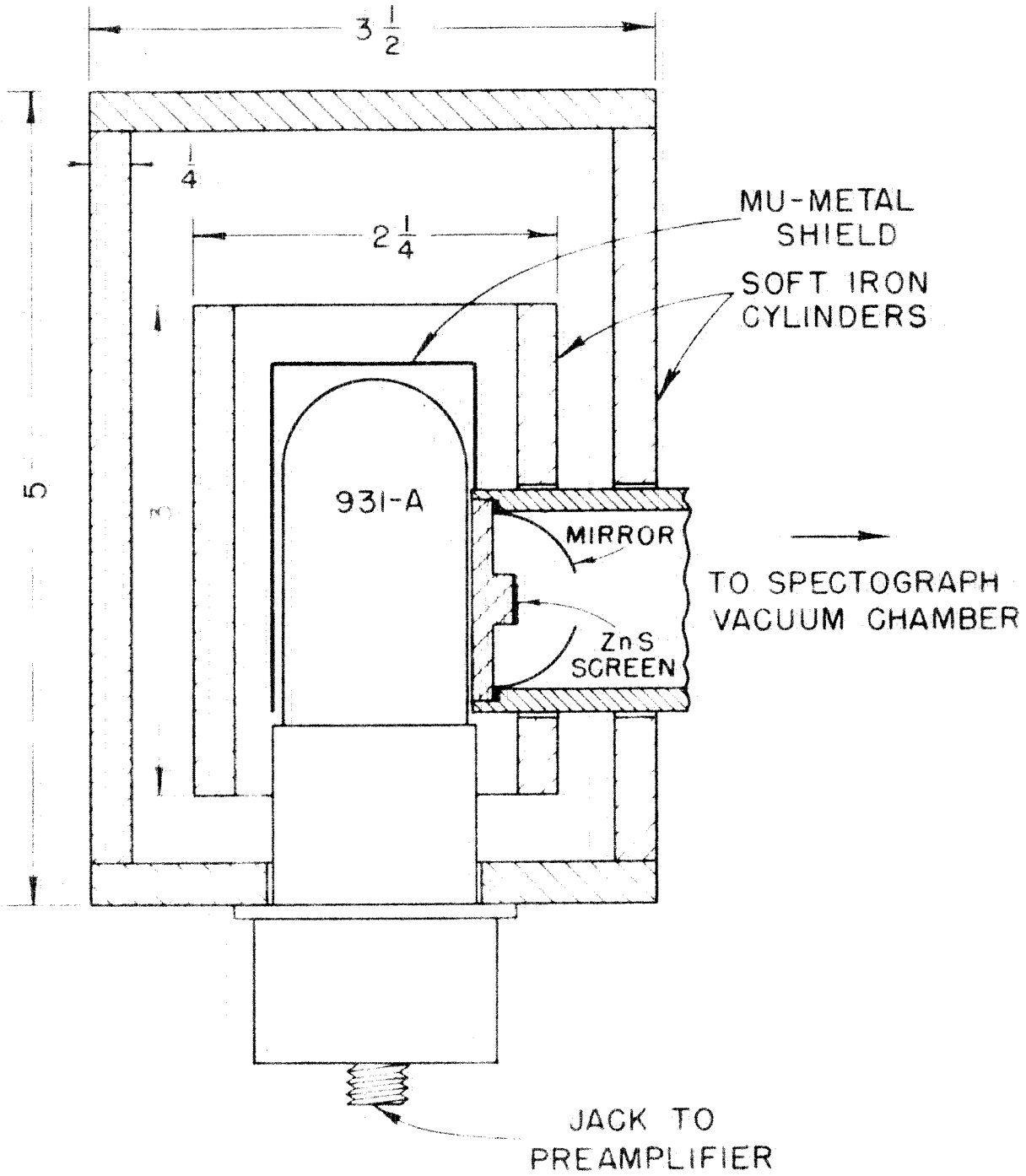

SCINTILLATION COUNTER

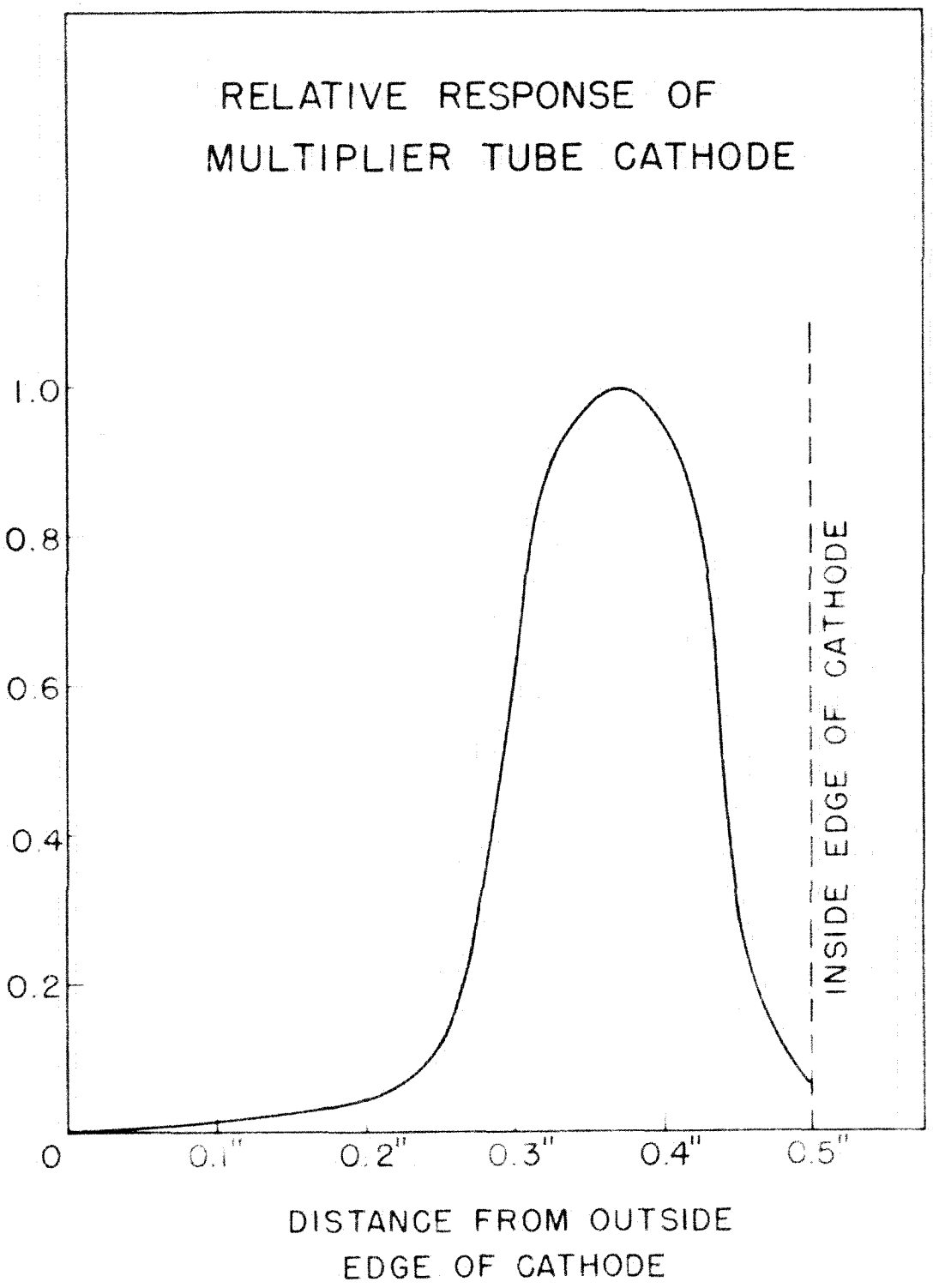
RELATIVE RESPONSE OF
MULTIPLIER TUBE CATHODE
1.0
0.8
0.6
0.4
0.2
0
0.1"
0.2"
0.3"
0.4"
0.5"
INSIDE EDGE OF CATHODE
DISTANCE FROM OUTSIDE
EDGE OF CATHODE

Fig 3

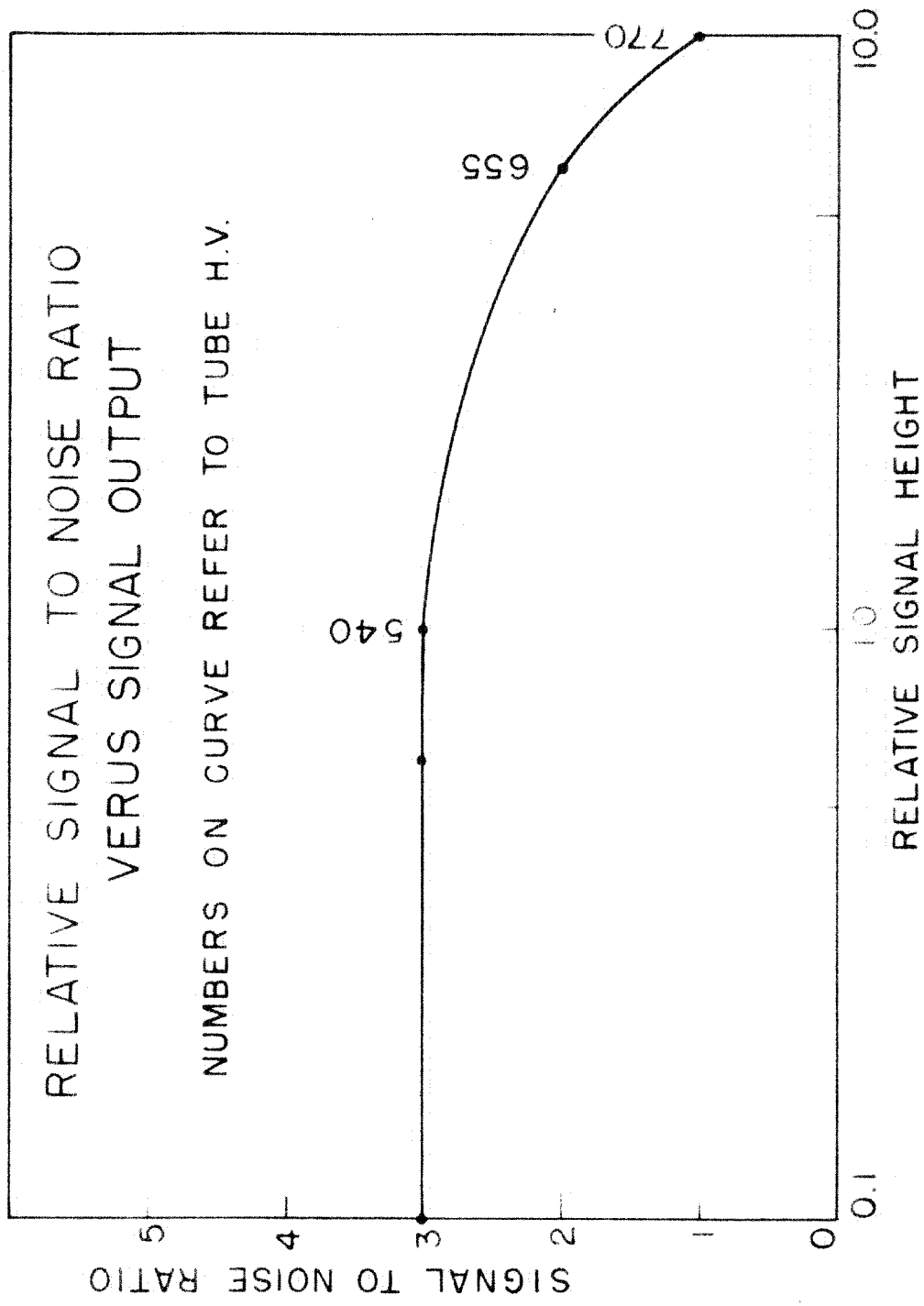
RELATIVE SIGNAL TO NOISE RATIO
VERUS SIGNAL OUTPUT
NUMBERS ON CURVE REFER TO TUBE H.V.
540
655
770
SIGNAL TO NOISE RATIO
0
1
2
3
4
5
0.1
1.0
10.0
RELATIVE SIGNAL HEIGHT

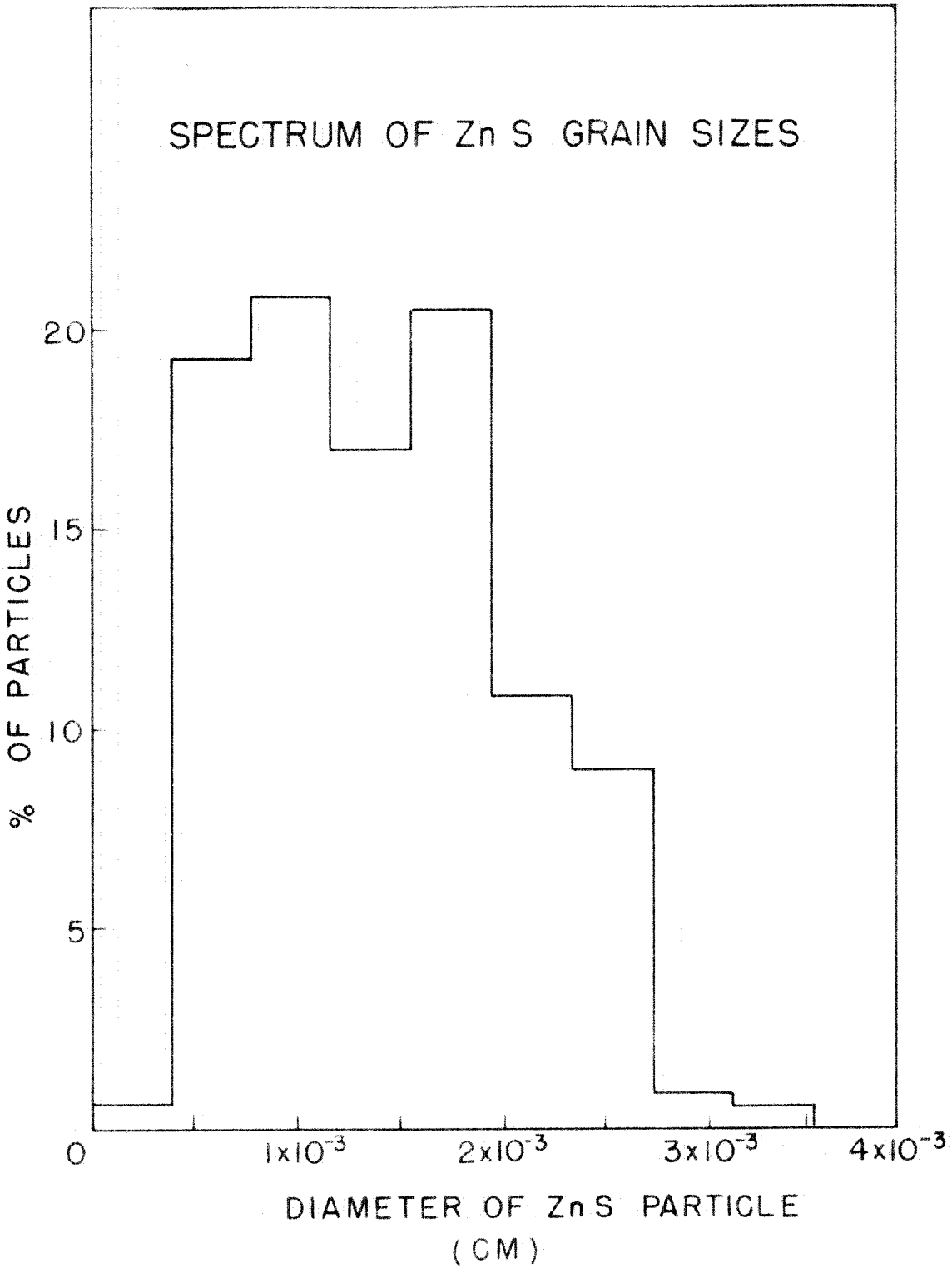
SPECTRUM OF Zn S GRAIN SIZES
% OF PARTICLES
20
15
10
5
0
1x10⁻³
2x10⁻³
3x10⁻³
4x10⁻³
DIAMETER OF Zn S PARTICLE
(CM)

Fig 7

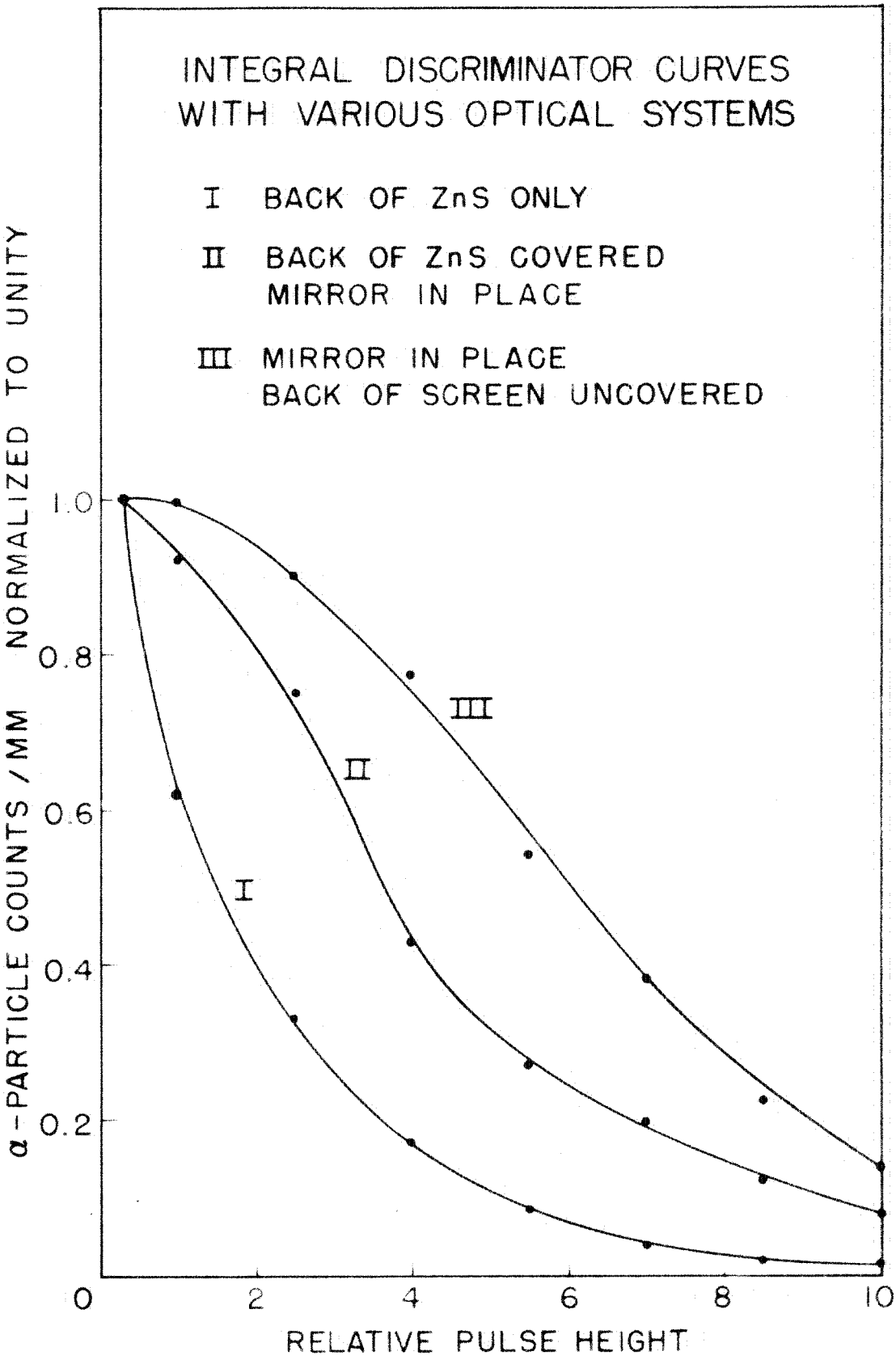
INTEGRAL DISCRIMINATOR CURVES
WITH VARIOUS OPTICAL SYSTEMS
I BACK OF ZnS ONLY
II BACK OF ZnS COVERED
MIRROR IN PLACE
III MIRROR IN PLACE
BACK OF SCREEN UNCOVERED
α-PARTICLE COUNTS / MM NORMALIZED TO UNITY
1.0
0.8
0.6
0.4
0.2
0
2
4
6
8
10
RELATIVE PULSE HEIGHT
I
II
III

DWG. NO.

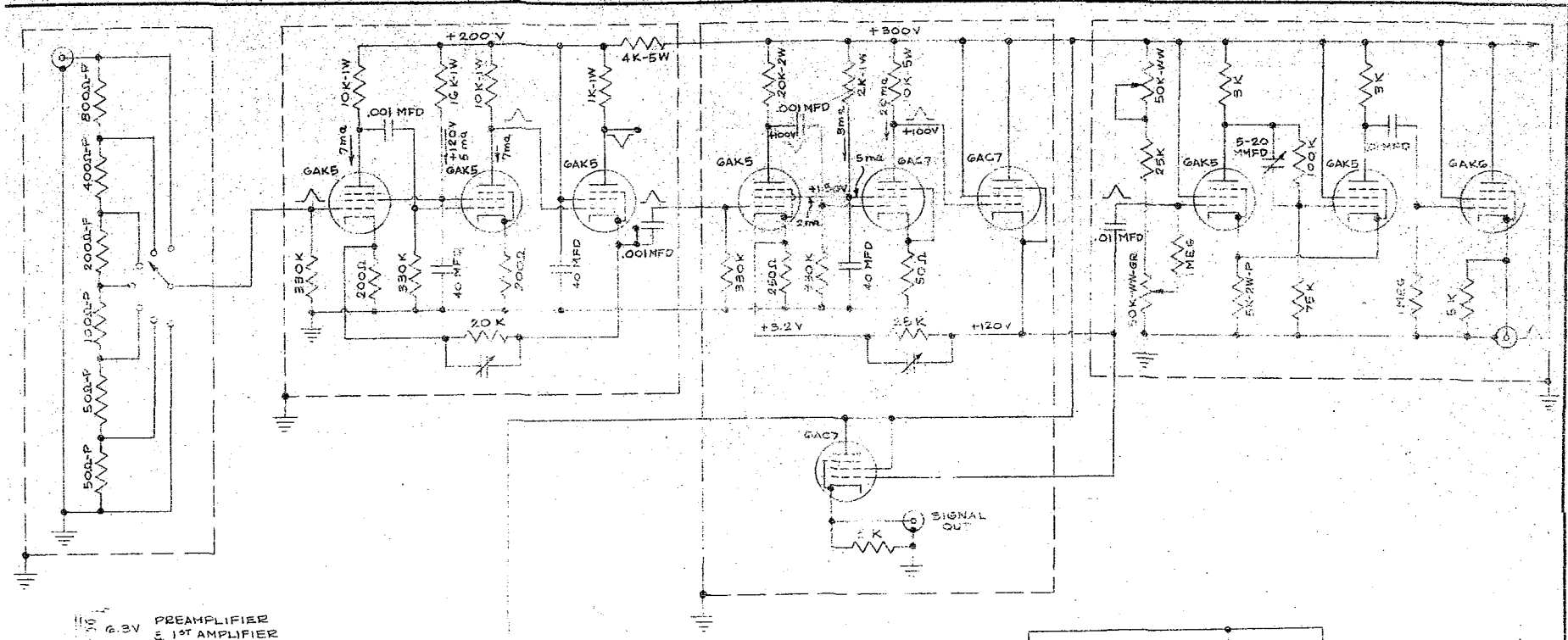

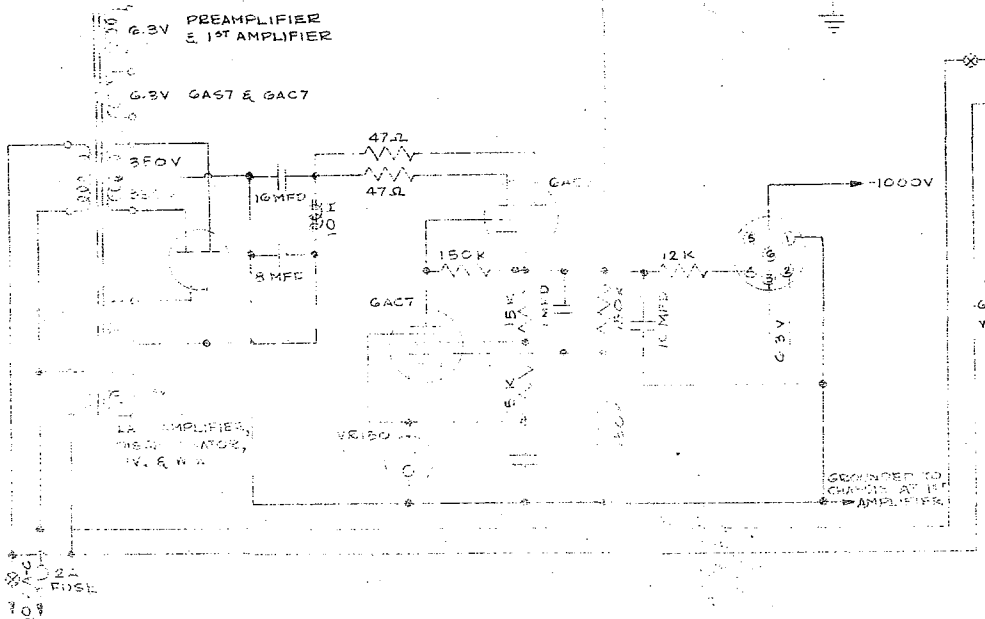

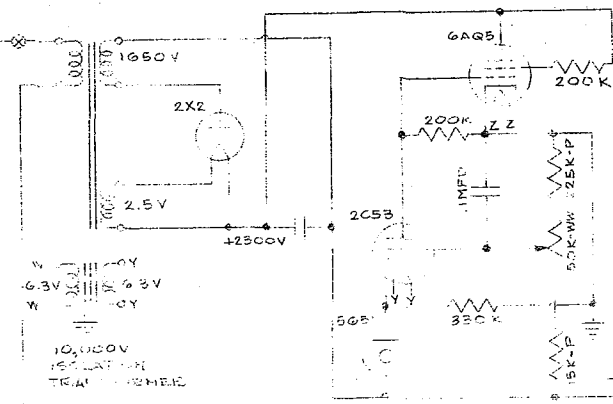

MATL.	NAME KR 100A PULSE AMPLIFIER		DWG NO.
NO. REQD	UNIT CIRCUIT SCHEMATIC		DATE 3-10-1950
TOL. UNLESS SPECIFIED ±	CALIFORNIA INSTITUTE OF TECHNOLOGY OEMsr. 418		FILE
HEAT TREAT.			SCALE
FINISH	WEIGHT	DRAWN BY	CHECKED BY
A	B	C	F
E	F	G	H

FORM 304

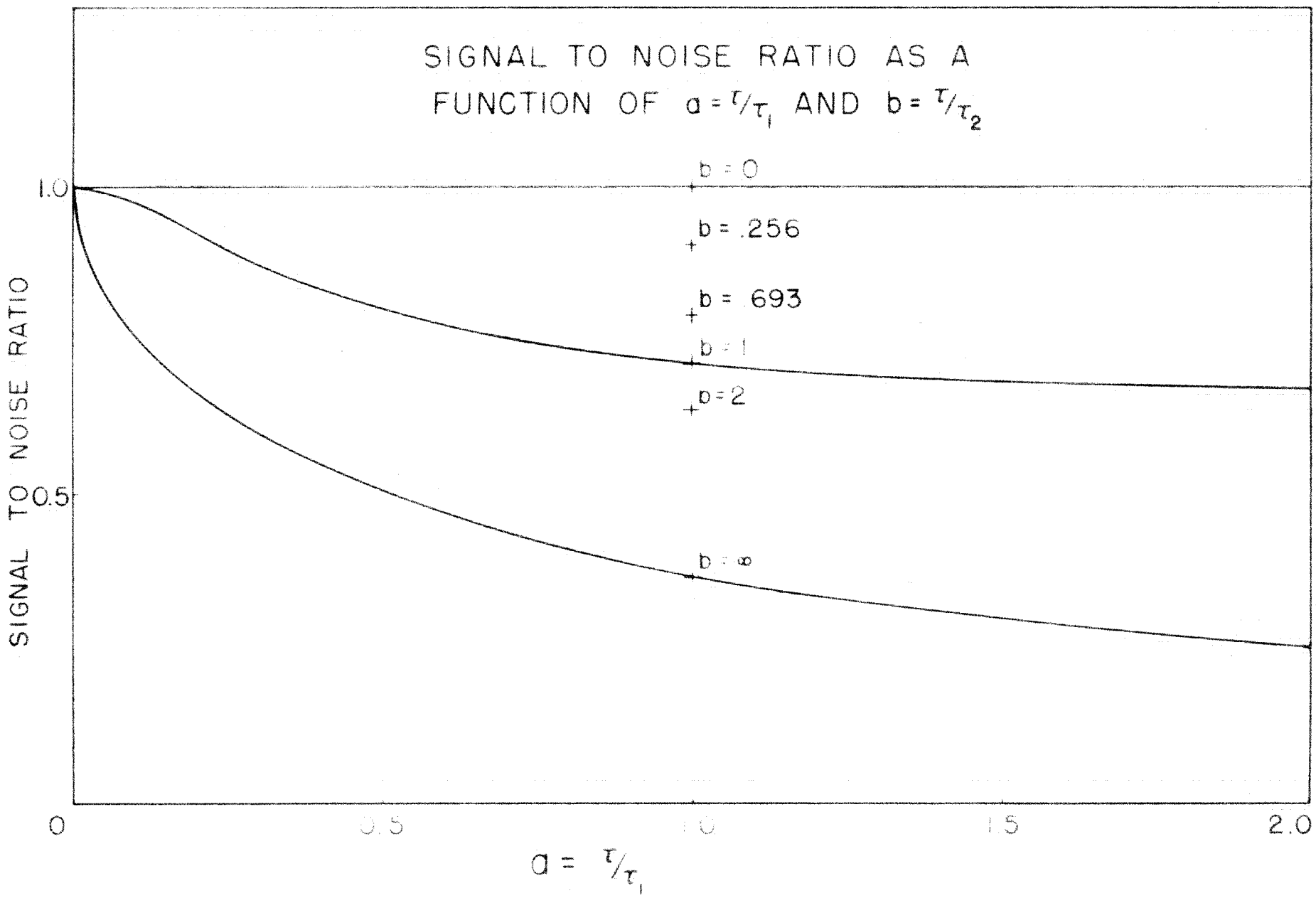
SIGNAL TO NOISE RATIO AS A
FUNCTION OF a = τ/τ1 AND b = τ/τ2
b = 0
b = .256
b = .693
b = 1
b = 2
b = ∞
SIGNAL TO NOISE RATIO
1.0
0.5
0
0.5
1.0
1.5
2.0
a = τ/τ1

Fig 10

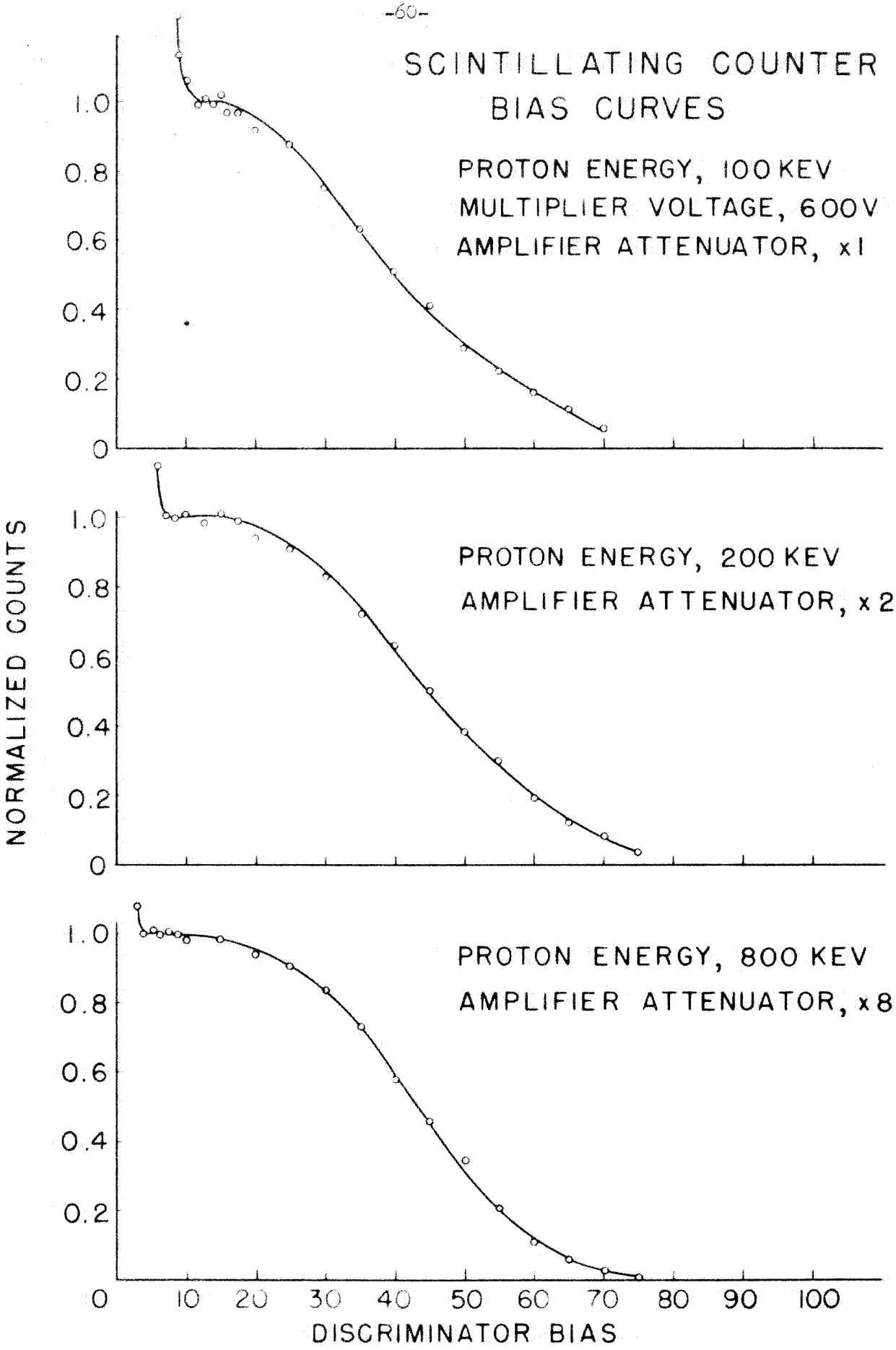
SCINTILLATING COUNTER
BIAS CURVES
PROTON ENERGY, 100 KEV
MULTIPLIER VOLTAGE, 600V
AMPLIFIER ATTENUATOR, x1
PROTON ENERGY, 200 KEV
AMPLIFIER ATTENUATOR, x2
PROTON ENERGY, 800 KEV
AMPLIFIER ATTENUATOR, x8
NORMALIZED COUNTS
0
0.2
0.4
0.6
0.8
1.0
10
20
30
40
50
60
70
80
90
100
DISCRIMINATOR BIAS

Fig 11

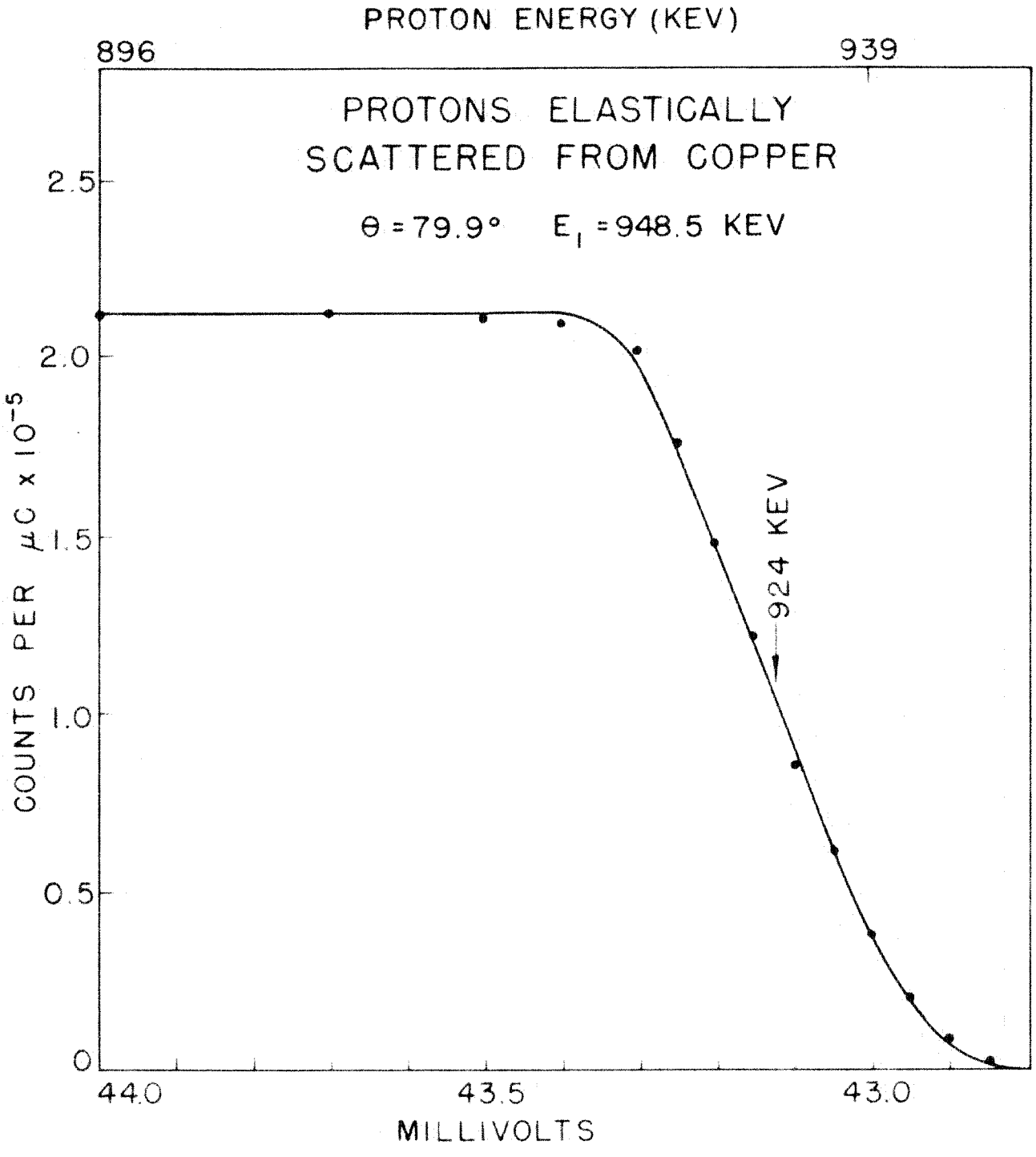
PROTON ENERGY (KEV)
896
939
PROTONS ELASTICALLY
SCATTERED FROM COPPER
θ = 79.9° E1 = 948.5 KEV
924 KEV
COUNTS PER μC x 10⁻⁵
2.5
2.0
1.5
1.0
0.5
0
44.0
43.5
43.0
MILLIVOLTS

Fig 12

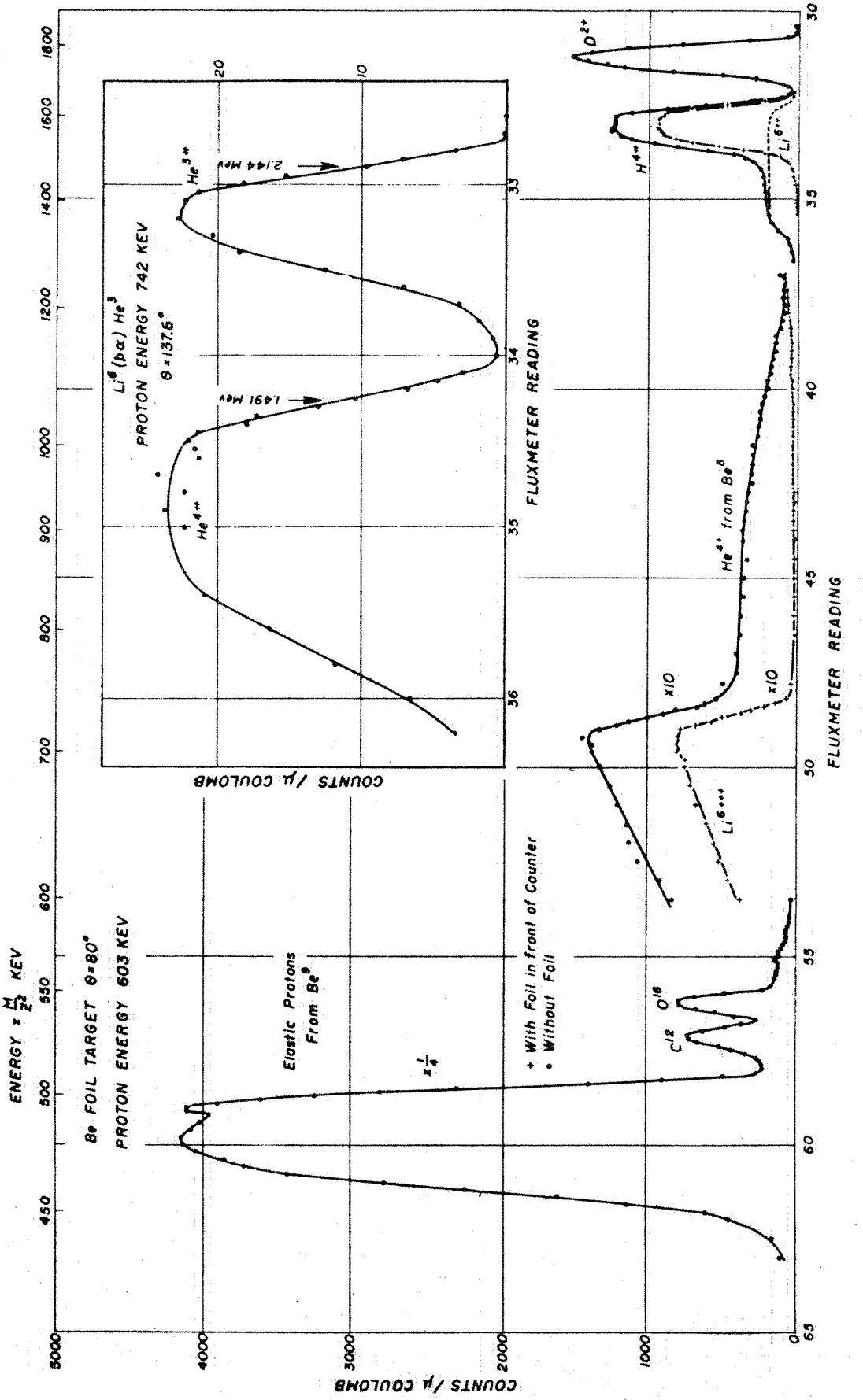
ENERGY x M/Z² KEV
Be FOIL TARGET θ=80°
PROTON ENERGY 603 KEV
Elastic Protons From Be⁹
x 1/4
+ With Foil in front of Counter
• Without Foil
C¹² O¹⁶
Li⁶⁺⁺⁺
x10
x10
He⁴⁺ from Be⁸
H⁴⁺
D²⁺
Li⁶⁺⁺
FLUXMETER READING
COUNTS / μ COULOMB
Li⁶(dα) He³
PROTON ENERGY 742 KEV
θ=137.6°
2.144 MeV
1.491 MeV
He³⁺⁺
He⁴⁺⁺
FLUXMETER READING
COUNTS / μ COULOMB

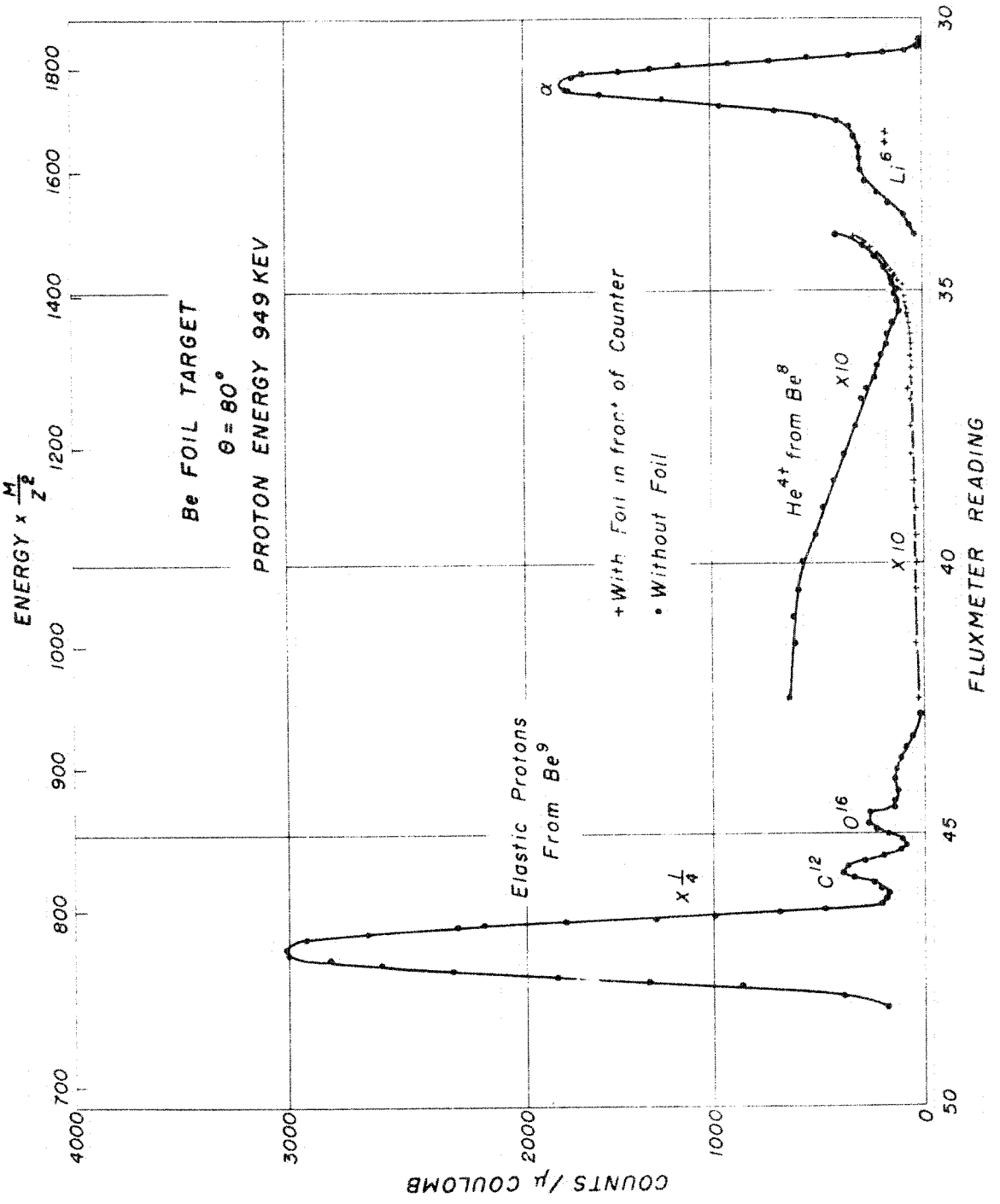
ENERGY x M/Z²
Be FOIL TARGET
θ = 80°
PROTON ENERGY 949 KEV
+ With Foil in front of Counter
• Without Foil
Elastic Protons From Be⁹
x 1/4
C¹²
O¹⁶
He⁴ from Be⁸
X10
X10
α
Li⁶⁺⁺
COUNTS / μ COULOMB
FLUXMETER READING
4000
3000
2000
1000
0
700
800
900
1000
1200
1400
1600
1800
50
45
40
35
30

Fig 14

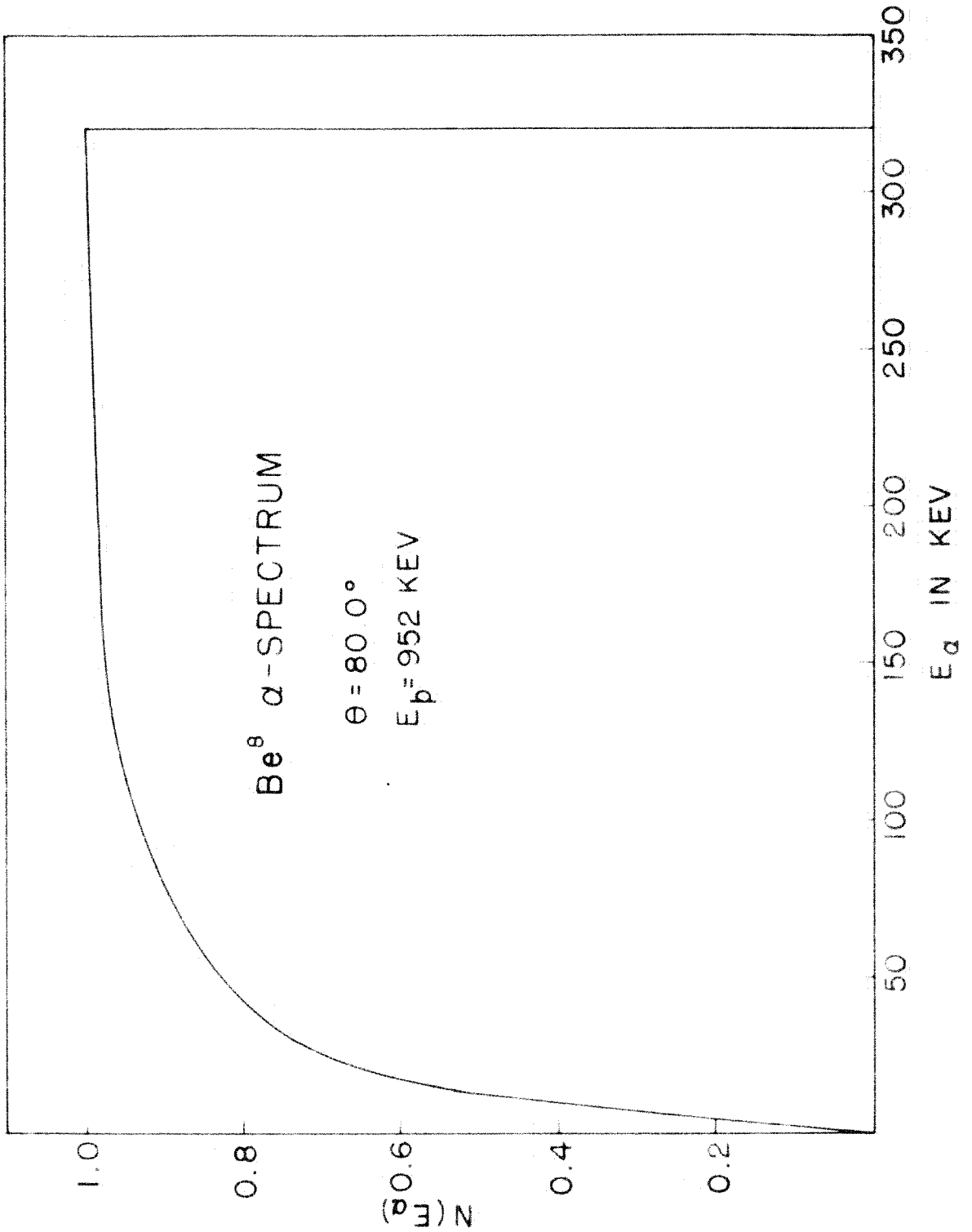
Be⁸ α-SPECTRUM
θ = 80.0°
E_b = 952 KEV
N(E_α)
1.0
0.8
0.6
0.4
0.2
50
100
150
200
250
300
350
E_α IN KEV

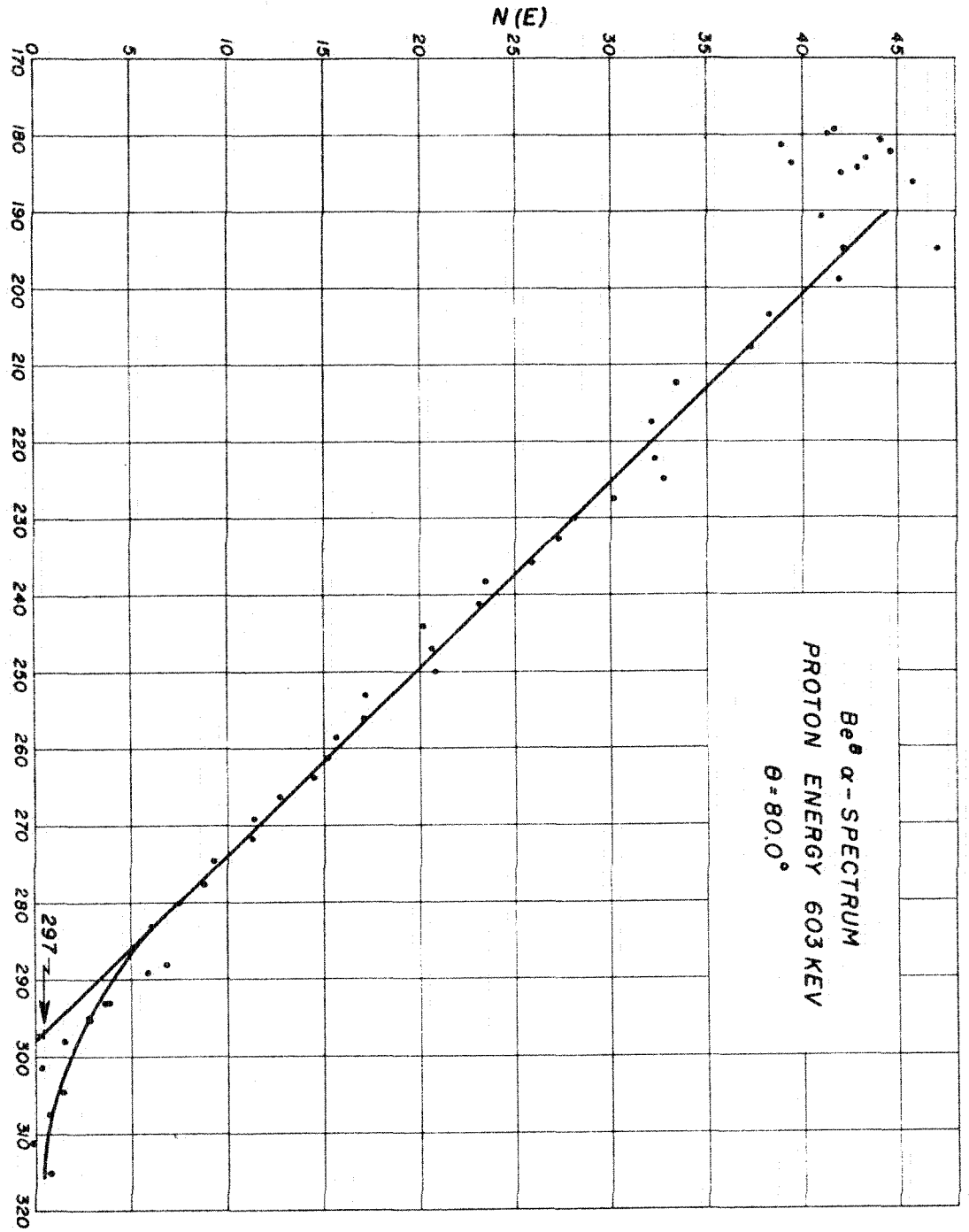
N(E)
0
5
10
15
20
25
30
35
40
45
170
180
190
200
210
220
230
240
250
260
270
280
290
300
310
320
297
Be⁸ α-SPECTRUM
PROTON ENERGY 603 KEV
θ=80.0°
α PARTICLE ENERGY IN KEV

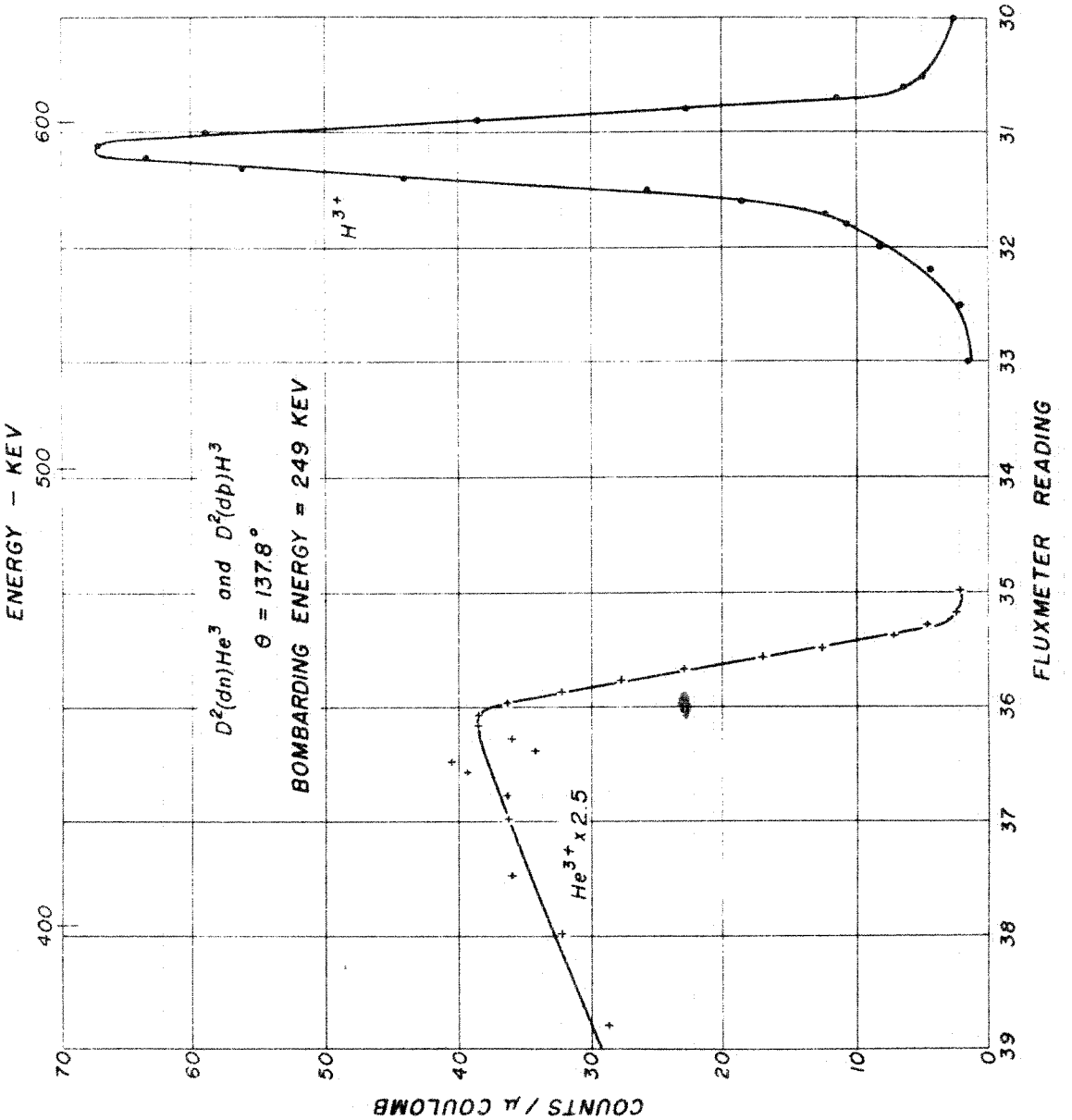
ENERGY - KEV
400
500
600
$D^2(dn)He^3$ and $D^2(dp)H^3$
θ = 137.8°
BOMBARDING ENERGY = 249 KEV
H^{3+}
He^{3+} x 2.5
COUNTS / μ COULOMB
70
60
50
40
30
20
10
0
FLUXMETER READING
30
31
32
33
34
35
36
37
38
39